

DIPLOMARBEIT

Classical Boundary Layer Behavior in the Vicinity of a Curvature Jump of the Wall Contour

ausgeführt zum Zwecke der Erlangung des akademischen Grades eines
Diplom-Ingenieurs unter der Leitung von

Ao.Univ.Prof. Dipl.-Ing. Dr.techn. Stefan Braun
E322 - Institut für Strömungsmechanik und Wärmeübertragung

eingereicht an der Technischen Universität Wien
Fakultät für Maschinenwesen und Betriebswissenschaften

von

Jarmila Vodinská
0426167
Döblinger Hauptstraße 20/1/11
1190 Wien

Wien, November 2014

.....

This work is dedicated to the memory of my father.

Abstract

Laminar flow past a parametrized family of semi-infinite thin bodies with adjustable curvature jump in their contour is investigated according to Prandtl's classical (first order) boundary layer theory. Accounting for the slenderness a perturbation ansatz is used to derive a potential flow solution as an approximation for the part of the surrounding flow, where viscosity effects can be neglected. The assumption of a slightly perturbed oncoming flow is violated in close vicinity of the leading edge stagnation point, where a local solution is found in an appropriately stretched coordinate system. Both solutions are combined in the spirit of matched asymptotic expansions using Van Dyke's matching rule to receive a uniformly valid approximation (compound solution) for the velocity distribution at the surface, which defines the prescribed pressure distribution along the viscous boundary layer in the immediate neighborhood of the solid wall. Finally, the boundary layer equations are derived and numerically solved for increasing strength of the curvature discontinuity at the surface. The break-down of the classical boundary layer theory is indicated by the occurrence of a Goldstein-singularity at the location of the curvature jump independent of its magnitude. This outcome suggests the application of advanced asymptotic concepts to the presented problem to account for the interaction between the boundary layer and the external flow (i. e. triple-deck theory).

Acknowledgments

I want to thank my adviser, Prof. Stefan Braun, for inducting me into this field of research and for his outstanding support and availability during the entire development of this work. Special thanks to Prof. Helmut Sobieczky for his highly contagious enthusiasm for aerodynamics and constructive help especially in the early beginnings of the present study. I wish to acknowledge the help provided by Prof. Herbert Steinrück. His willingness to give his time so generously has been very much appreciated during this and other projects.

I would like to extend my thanks specially to my mother, my sister and my life partner for offering me a great deal of encouragement over the many years of my studies.

Preface

When once you have tasted flight, you will forever walk the Earth with your eyes turned skyward, for there you have been, and there you will always long to return.

(Leonardo Da Vinci)

My specialization in the field of fluid mechanics is a consequence of my great passion for airplanes and interest in physics. I have first experienced piloting during a summer school for students of aviation and engineering in Italy organized by a small group of young, enthusiastic and passionate assistants around Prof. Andrea Alaimo¹, which has definitely ignited the spark.

New technologies in the air-vehicle industry such as morphing aircraft structures (in-flight shape-adjustments) require a reflective understanding of the fluid-mechanic phenomena responding to discontinuities of surface curvature (e.g. separation of flow, laminar-turbulent transition).

This initial study provides an access to the theory of matched asymptotic expansions and thus to the theoretical understanding of flow behavior whereas further studies may be concerned with the accordance or the complementarity of the theoretical findings and the solutions provided by modern CFD-solvers in which engineers often trust without the competence of a theoretical interpretation.

¹Kore University of Enna, Italy

Contents

1	Introduction	1
2	Definitions	3
2.1	Dimensionless quantities and governing equations	3
2.2	The thickness-function	5
3	Potential flow past thin airfoil	7
3.1	Potential theory	7
3.2	Thin airfoil expansion	7
3.3	Solution of the thin airfoil problem by distribution of singularities .	10
3.4	Matching with a local solution near sharp edge	13
3.4.1	Inner variables	13
3.4.2	Inner solution	14
3.4.2.1	Transformation of the Laplace equation	14
3.4.2.2	Separation of variables	17
3.4.2.3	Solution and boundary conditions	18
3.4.3	Van Dyke's matching rule	19
3.5	Compound solution	22
4	Behavior of the boundary layer	29
4.1	First order boundary layer theory	29
4.2	Derivation of the Prandtl equation	29
4.2.1	Falkner-Skan equation	32
4.3	Numerical solution of the Prandtl equation	34
4.4	Presentation of the results	35
5	Conclusion and outlook	44
	Bibliography	45

1 Introduction

In this academic work a two-dimensional laminar flow of a viscous fluid past a smooth surface showing a curvature discontinuity is studied. Assuming high Reynolds numbers *Prandtl's classical (first order) boundary layer theory* is applied and thus the flow is split into two regions: a very thin layer in proximity of the surface (*boundary layer*), where viscosity of the flow plays an important role, and the surrounding region (outside of the boundary layer), where viscous forces can be neglected compared to inertia forces, the *potential flow*. The latter defines the pressure along the main stream direction in the thin viscous layer and hence represents a boundary condition at the interface, where the two velocity distributions must match. The derivation of an adequate approximation for the inviscid velocity- and thus the pressure-distribution for different regions of the flow surrounding the boundary layer was the objective of a preliminary project study and is also included in this work.

A detailed investigation is done for a family of thin half-bodies represented by a monotonically growing parametrized function $\tau T(x; \varepsilon(k))$ with a *thickness-to-ramp-length ratio* $\tau \ll 1$ within a unity square with $T(x = 0) = 0$, $T(x = 1) = 1$ and with $T'(x = 1) = 0$. The curvature parameter $\varepsilon(k)$ defines the curvature k of $T(x)$ at $x = 1$ and thus creates a family of *thickness-functions*

$$y(x; \tau, k) = \tau T(x; \varepsilon(k)) \tag{1.1}$$

with an adjustable magnitude of the curvature jump at $x = 1$, if we assume that these curves are joined to a straight horizontal line at this point to create the top side of a symmetrical half-body, Figure 2.1.

Dimensional and non-dimensional quantities are strictly distinguished throughout the entire study. Therefore all dimensional variables are denoted with a tilde. The definitions of dimensionless quantities and the characteristic dimensions of the present problem are summarized in chapter 2.

According to *potential theory*, the motion of a steady, incompressible, and irrotational planar flow is governed by the *Laplace equation*. Even though it is the simplest linear elliptic partial differential equation, it may be difficult to find an

1 Introduction

accurate solution for the given boundary conditions. In the present case, according to *thin airfoil theory*, we can approximate the solution through asymptotic expansion in powers of the thickness parameter, τ . As τ tends to zero, the limiting solution is the unperturbed parallel flow. This approach is only valid, if we assume small disturbances of the unperturbed flow. It is obvious that this assumption is violated at the leading edge at $x = 0$, where the velocity is zero (*stagnation point*). Therefore one has to find a local solution near the leading edge to obtain a uniformly valid flow field description by means of *matched asymptotic expansions*.

In this study we concentrate on the leading order effects of τ , but it is described how to proceed to higher order approximations. Furthermore, all calculations refer to the top side of the symmetrical half-body. One can obtain the results for the bottom side simply by setting $T(x) \rightarrow -T(x)$.

The non-linear, partial differential equations describing the viscous layer (*boundary layer equations*) are solved numerically and the shear stress distributions at the surface are derived for the defined half-body to study the effects of a curvature jump of the contour on the viscous layer. Moreover the displacement thickness of the boundary layer for the different curves is computed. A particular aim lies on the observation of the Goldstein-singularity at $x = 1$ as the curvature jump is slightly increased starting from zero.

2 Definitions

2.1 Dimensionless quantities and governing equations

Considering semi-infinite bodies, first of all, we have to decide how to define a characteristic length. In the present case we investigate the behavior of the surrounding flow especially in the vicinity of a curvature jump and therefore it is convenient to locate it at $x = 1$. As the analyzed half-bodies are set up of a non-linear ramp, which is merged with a strait horizontal line to provoke the discontinuity, we use the ramp-length, \tilde{L} , as shown in Figure 2.1, as a reference and scale the x - and y -variables according to

$$x = \frac{\tilde{x}}{\tilde{L}}, \quad y = \frac{\tilde{y}}{\tilde{L}}. \quad (2.1)$$

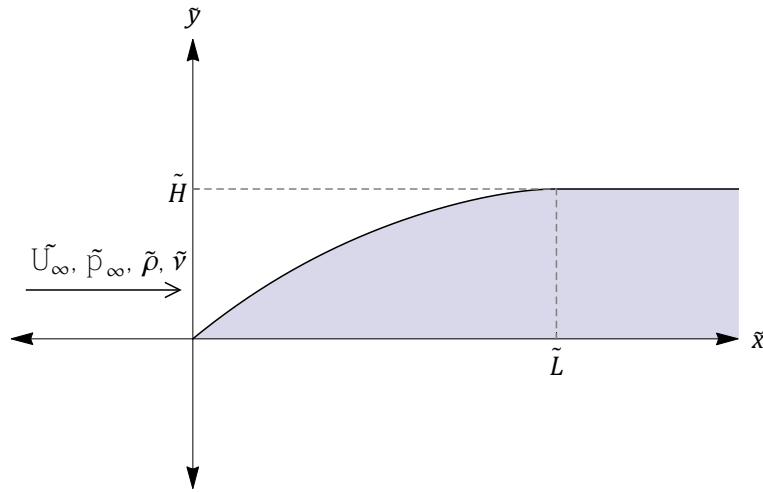


Figure 2.1: Geometrical set up of the flow: characteristic dimensions and quantities.

2 Definitions

Assuming a thin half-body, we define the thickness-to-ramp-length ratio, τ , as

$$\tau = \frac{\tilde{H}}{\tilde{L}} \ll 1. \quad (2.2)$$

The unperturbed free-stream velocity \tilde{U}_∞ is used as reference velocity¹, i. e.

$$\vec{q} = \begin{pmatrix} u \\ v \end{pmatrix} = \frac{\vec{\tilde{q}}}{\tilde{U}_\infty} = \frac{1}{\tilde{U}_\infty} \begin{pmatrix} \tilde{u} \\ \tilde{v} \end{pmatrix}. \quad (2.3)$$

We obtain the dimensionless form of the governing Navier-Stokes equations, as

$$\text{Continuity equation:} \quad \vec{\nabla} \cdot \vec{q} = 0, \quad (2.4a)$$

$$\text{Equation of motion:} \quad \left(\vec{q} \cdot \vec{\nabla} \right) \vec{q} = -\vec{\nabla} p + \frac{1}{Re} \Delta \vec{q}, \quad (2.4b)$$

if we assume a steady, incompressible, Newtonian fluid with the constant viscosity $\tilde{\nu}$ and the constant density $\tilde{\rho}$. Furthermore, Re denotes the Reynolds number

$$Re = \frac{\tilde{U}_\infty \tilde{L}}{\tilde{\nu}} \ll 1, \quad (2.5)$$

assumed to be high and p the scalar pressure, non-dimensionalized by

$$p = \frac{\tilde{p} - \tilde{p}_\infty}{\tilde{\rho} \tilde{U}_\infty^2}. \quad (2.6)$$

It is shown in chapter 4, how to derive the boundary layer equations from the Navier-Stokes equations. Obviously, assuming an irrotational flow and $Re \rightarrow \infty$ we obtain the potential flow equations for the approximation of the external flow as

$$\text{Continuity equation:} \quad \vec{\nabla} \cdot \vec{q} = 0, \quad (2.7a)$$

$$\text{Vorticity of the flow field:} \quad \vec{\nabla} \times \vec{q} = 0, \quad (2.7b)$$

whereby (2.4b) turns into the *Euler equation* for the present case, written as

$$\left(\vec{q} \cdot \vec{\nabla} \right) \vec{q} = -\vec{\nabla} p, \quad (2.8)$$

which is valid within the whole potential flow field (see e. g. [3]).

¹In this study we have to distinguish between the velocity field of the potential flow and the one within the boundary layer, which is denoted with the index b , but the scaling presented in this chapter remains valid for both.

2.2 The thickness-function

We consider symmetrical semi-infinite bodies, Figure 2.2, described by $y = \pm\tau T(x; \varepsilon(k))$, where $T(x; \varepsilon(k))$ is the parametrized *thickness-function* of order unity, τ the thickness-to-ramp-length ratio according to (2.2) and $\varepsilon(k)$ a *curvature parameter*.

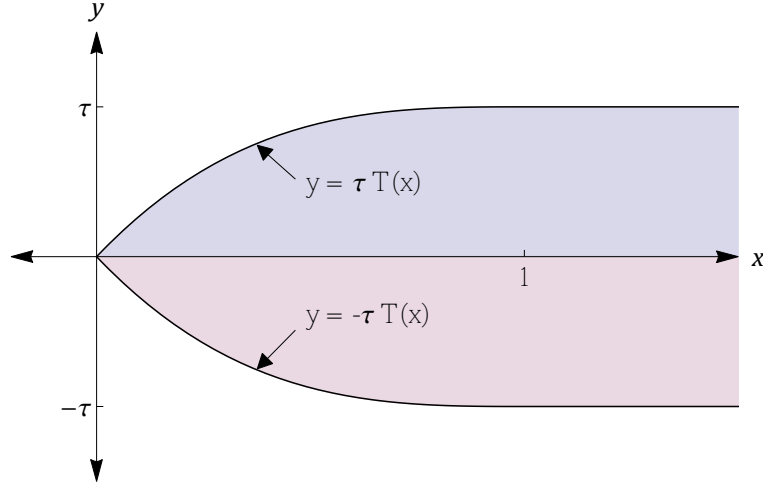


Figure 2.2: Semi-infinite thin body.

The thickness-function $T(x; \varepsilon)$, shown in Figure 2.3, is defined within the unity square as

$$T(x; \varepsilon) = \varepsilon [1 - (1 - x)^3] + \frac{(1 - \varepsilon)x [2\varepsilon - (\varepsilon + 1)x + 1]}{\varepsilon - x + 1}, \quad 0 < \varepsilon < 1. \quad (2.9)$$

The curvature parameter $\varepsilon = \varepsilon(k)$ gives the possibility to define the curvature k of the ramp-function $T(x)$ at $x = 1$ and thus to vary the magnitude of the curvature discontinuity at the point, where the ramp-function meets the horizontal line. It is given by

$$\varepsilon(k) = \frac{1}{4}(k + \sqrt{16 + k^2}), \quad (2.10)$$

since k is defined as

$$T''(x = 1) =: k. \quad (2.11)$$

As $\varepsilon(k)$ does not depend on x , we can treat it here as a constant, keeping in mind, that $0 < \varepsilon < 1$ with $\varepsilon(0) = 1$ and $\lim_{k \rightarrow -\infty} \varepsilon(k) = 0$.

2 Definitions

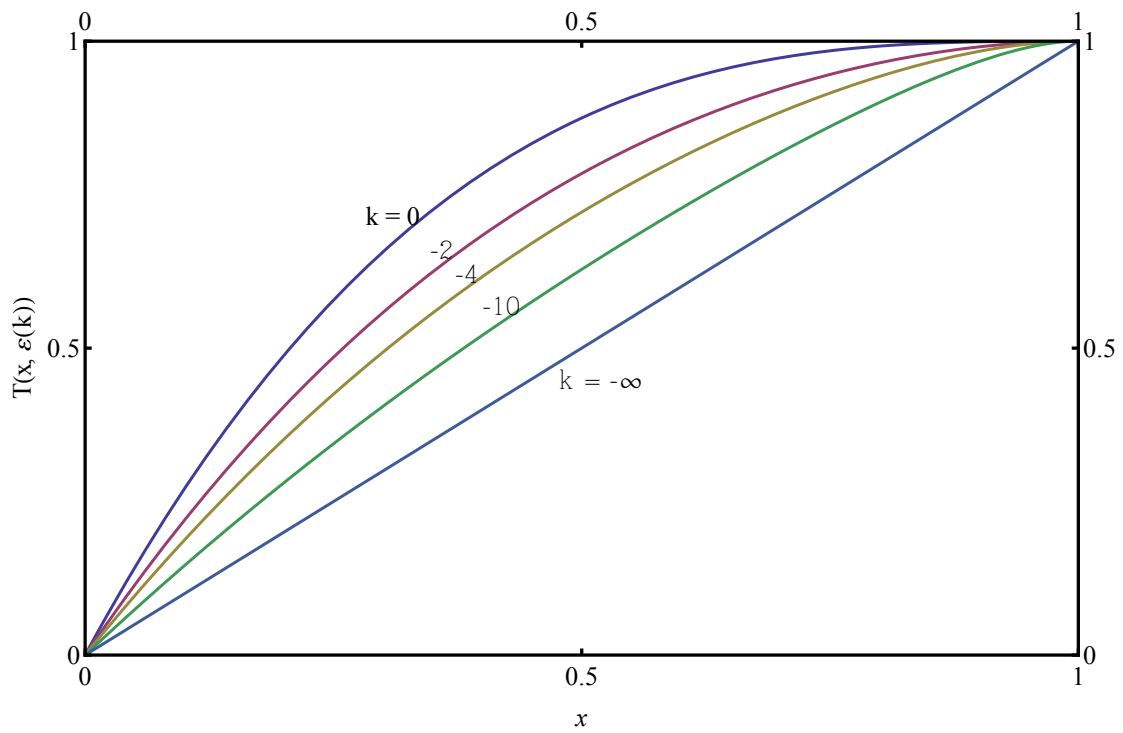


Figure 2.3: Ramp-functions according to (2.9) for different curvatures k at $x = 1$.

3 Potential flow past thin airfoil

3.1 Potential theory

Potential theory is applicable, if we assume (incompressible and) irrotational flow and exclude thermal effects. In such a case, there exists a scalar function called *velocity potential* ϕ , which satisfies $\vec{q} = \vec{\nabla}\phi$, where \vec{q} denotes the *velocity field*. In combination with (2.4a) we obtain the *Laplace equation*

$$\Delta\phi = 0. \quad (3.1)$$

In the present case of the semi-infinite body the full problem consists of the Laplace equation and two boundary conditions, the unperturbed free-stream condition in the far field and the tangency condition at the surface of the half-body. Hence we have

$$\text{Laplace equation: } \phi_{xx} + \phi_{yy} = 0, \quad (3.2)$$

$$\text{unperturbed free-stream condition: } \phi \sim x + o(1) \quad \text{as } x^2 + y^2 \rightarrow \infty, \quad (3.3)$$

$$\text{tangency condition: } \frac{\phi_y}{\phi_x} = \tau T'(x) \quad \text{as } y = \pm\tau T(x). \quad (3.4)$$

3.2 Thin airfoil expansion

The slenderness of the half-body causes only small perturbations to the free stream and therefore allows for an expansion of the potential about the undisturbed flow state. Hence we interpret the solution of the problem given in (3.2)-(3.4) as a linear combination of the potential of the uniform parallel flow plus some perturbation potential. With τ as the perturbation parameter and $\varphi_j(x, y)$, with $j = 1, 2, \dots$, as the j -th order perturbation potential of order $O(1)$ the asymptotic expansion is given by

$$\phi(x, y) = x + \tau\phi_1(x, y) + \tau^2\phi_2(x, y) + \dots, \quad (3.5)$$

3 Potential flow past thin airfoil

with the partial derivatives

$$u = \phi_x(x, y) \sim 1 + \tau\phi_{1x}(x, y) + \tau^2\phi_{2x}(x, y) + \dots, \quad (3.6)$$

$$v = \phi_y(x, y) \sim \tau\phi_{1y}(x, y) + \tau^2\phi_{2y}(x, y) + \dots \quad (3.7)$$

We need to apply this ansatz to the tangency condition at the half-body surface. Still the slenderness of the body gives occasion to a simplification. The thinness implies that the surface, where the tangency condition is given, is in close vicinity to the x -axis. Therefore, we Taylor expand (3.4) to obtain an approximation of the boundary condition on the surface. Of course we have to be aware of the nonuniformities as a consequence of these expansions.

Expanding ϕ_y for $y = \tau T(x) \ll 1$ we get

$$\begin{aligned} \phi_y(x, \tau T(x)) \sim & \tau \left[\phi_{1y}(x, 0) + \phi_{1yy}(x, 0)\tau T(x) + \frac{1}{2}\phi_{1yyy}(x, 0)(\tau T(x))^2 + \dots \right] \\ & + \tau^2 \left[\phi_{2y}(x, 0) + \phi_{2yy}(x, 0)\tau T(x) + \frac{1}{2}\phi_{2yyy}(x, 0)(\tau T(x))^2 + \dots \right] + \dots, \end{aligned} \quad (3.8)$$

which, after rearranging in powers of τ yields

$$\phi_y(x, \tau T(x)) \sim \tau\phi_{1y}(x, 0) + \tau^2 [\phi_{1yy}(x, 0)T(x) + \phi_{2y}(x, 0)] + \dots \quad (3.9)$$

Analogously, expanding ϕ_x for $y = \tau T(x) \ll 1$, we obtain

$$\begin{aligned} \phi_x(x, \tau T(x)) \sim & 1 + \tau \left[\phi_{1x}(x, 0) + \phi_{1xy}(x, 0)\tau T(x) + \frac{1}{2}\phi_{1xyy}(x, 0)(\tau T(x))^2 + \dots \right] \\ & + \tau^2 \left[\phi_{2x}(x, 0) + \phi_{2xy}(x, 0)\tau T(x) + \frac{1}{2}\phi_{2xyy}(x, 0)(\tau T(x))^2 + \dots \right] + \dots, \end{aligned} \quad (3.10)$$

and

$$\phi_x(x, \tau T(x)) \sim 1 + \tau\phi_{1x}(x, 0) + \tau^2 [\phi_{1xy}(x, 0)T(x) + \phi_{2x}(x, 0)] + \dots \quad (3.11)$$

We insert (3.9) and (3.11) into the tangency condition (3.4) to get

$$T'(x) = \frac{\phi_{1y}(x, 0) + \tau [\phi_{1yy}(x, 0)T(x) + \phi_{2y}(x, 0)] + \dots}{1 + \tau\phi_{1x}(x, 0) + \tau^2 [\phi_{1xy}(x, 0)T(x) + \phi_{2x}(x, 0)] + \dots}. \quad (3.12)$$

Thus, for small τ the Taylor series expansion of (3.12) yields

$$\begin{aligned} T'(x) &= [\phi_{1y}(x, 0) + \tau(\phi_{1yy}(x, 0)T(x) + \phi_{2y}(x, 0)) + O(\tau^2)] [1 - \tau\phi_{1x}(x, 0) + O(\tau^2)] \\ &= \phi_{1y}(x, 0) + \tau [\phi_{1yy}(x, 0)T(x) + \phi_{2y}(x, 0) - \phi_{1y}(x, 0)\phi_{1x}(x, 0)] + O(\tau^2). \end{aligned} \quad (3.13)$$

3 Potential flow past thin airfoil

Equating coefficients in equal powers of τ leads to a sequence of problems comprising the Laplace equation and two boundary conditions (1. tangency condition, which is now linear and 2. the unperturbed free-stream condition) for each order of τ :

Order τ^0 :

$$\text{Laplace equation:} \quad \phi_{1xx} + \phi_{1yy} = 0 \quad (3.14a)$$

$$1. \ x^2 + y^2 \rightarrow \infty: \quad \phi_1 \rightarrow 0 \quad (3.14b)$$

$$2. \ y = 0: \quad \phi_{1y}(x, 0) = T'(x) \equiv T'_1(x) \quad (3.14c)$$

Order τ^1 :

$$\text{Laplace equation:} \quad \phi_{2xx} + \phi_{2yy} = 0 \quad (3.15a)$$

$$1. \ x^2 + y^2 \rightarrow \infty: \quad \phi_2 \rightarrow 0 \quad (3.15b)$$

$$2. \ y = 0, \text{ using (3.14c):} \quad \frac{\phi_{1yy}(x, 0)T(x) + \phi_{2y}(x, 0)}{\phi_{1x}(x, 0)} = T'(x)$$

$$\phi_{2y}(x, 0) = T'(x)\phi_{1x}(x, 0) - T(x)\phi_{1yy}(x, 0)$$

... we use (3.14a) to get

$$\phi_{2y}(x, 0) = T'(x)\phi_{1x}(x, 0) + T(x)\phi_{1xx}(x, 0)$$

$$\phi_{2y}(x, 0) = [T(x)\phi_{1x}(x, 0)]' \equiv T'_2(x) \quad (3.15c)$$

We can proceed in the same way to any higher order of τ and using the differential equations as well as the tangency conditions from previous order problems, we will always receive the first order problem with the only difference, that instead of the original thickness-function $T(x)$ the new problem will contain some modified thickness-function $T_n(x)$. The derivation of the next order problem ($O(\tau^2)$) can be found in e. g. [10].

3.3 Solution of the thin airfoil problem by distribution of singularities

Linearity of the Laplace equation implies that any linear combination of solutions is again a solution (superposition principle). Thus, we can describe more general flow fields combining well-known solutions such as, for example, sources and sinks. Distributing such singularities along the x -axis and interpreting the streamlines as the surface of a solid body, the flow field around any desired form can be obtained. Therefore, if the particular source/sink strengths are chosen accordingly and distributed between $x = 0$ and $x = 1$, we can also obtain the exact form of any of the half-bodies $T_n(x)$, $n = 1, 2, \dots$ derived in (3.2).

First, we consider the contribution $d\phi_n$ of a source at $x = \xi$ and $y = 0$ with a differential strength ds , given by

$$d\phi_n(x, y) = \frac{ds}{2\pi} \ln \sqrt{(x - \xi)^2 + y^2}. \quad (3.16)$$

Defining the source distribution function $m(\xi)$ by

$$ds = \frac{ds}{d\xi} d\xi = m(\xi) d\xi, \quad (3.17)$$

and integrating over all the sources distributed along the x -axis between $x = 0$ and $x = 1$ yields

$$\phi_n(x, y) = \frac{1}{2\pi} \int_0^1 m(\xi) \ln \sqrt{(x - \xi)^2 + y^2} d\xi. \quad (3.18)$$

The unknown source distribution function $m(\xi)$ can be found using the tangency condition

$$\phi_{ny}(x, 0) = T'_n(x). \quad (3.19)$$

We calculate the partial derivatives of (3.18) as

$$\begin{aligned} \phi_{ny}(x, y) &= \frac{1}{2\pi} \int_0^1 m(\xi) \frac{1}{\sqrt{(x - \xi)^2 + y^2}} \frac{1}{2\sqrt{(x - \xi)^2 + y^2}} 2y d\xi \\ &= \frac{1}{2\pi} \int_0^1 m(\xi) \frac{y}{(x - \xi)^2 + y^2} d\xi, \end{aligned} \quad (3.20)$$

$$\begin{aligned} \phi_{nx}(x, y) &= \frac{1}{2\pi} \int_0^1 m(\xi) \frac{1}{\sqrt{(x - \xi)^2 + y^2}} \frac{1}{2\sqrt{(x - \xi)^2 + y^2}} 2(x - \xi) d\xi \\ &= \frac{1}{2\pi} \int_0^1 m(\xi) \frac{(x - \xi)}{(x - \xi)^2 + y^2} d\xi. \end{aligned} \quad (3.21)$$

3 Potential flow past thin airfoil

Thus, the tangency condition requires

$$\phi_{ny}(x, 0) = \lim_{y \rightarrow 0} \frac{1}{2\pi} \int_0^1 m(\xi) \frac{y}{(x - \xi)^2 + y^2} d\xi = T'_n(x). \quad (3.22)$$

As the function $y/[(x - \xi)^2 + y^2]$ tends to zero for every $\xi \neq x$ we can assume that $m(\xi)$ only contributes to the integral at $\xi = x$ and thus we can treat it as a constant with respect to ξ with the value $m(x)$ and write:

$$\phi_{ny}(x, 0) = \lim_{y \rightarrow 0} \frac{1}{2\pi} m(x) \int_{\xi=0}^{\xi=1} \frac{y}{(x - \xi)^2 + y^2} d\xi = T'_n(x) \quad (3.23)$$

This integral can be solved, using

$$\int \frac{1}{1 + \sigma^2} = \arctan(\sigma), \quad |x| < 1 \text{ and } [\arctan(\sigma)]_{-\infty}^{\infty} = \pi \quad (3.24)$$

and the following transformation of (3.23):

$$\sigma = \frac{(\xi - x)}{y}, \quad \frac{d\sigma}{d\xi} = \frac{1}{y}. \quad (3.25)$$

Whereas $\xi = y\sigma + x$ and $d\xi = yd\sigma$ inserted in (3.23) gives

$$\frac{1}{2\pi} m(x) \int_{\lim_{y \rightarrow 0} \sigma(\xi=0)}^{\lim_{y \rightarrow 0} \sigma(\xi=1)} \frac{1}{1 + \sigma^2} d\sigma = \frac{1}{2\pi} m(x) \int_{-\infty}^{\infty} \frac{1}{1 + \sigma^2} d\sigma = \frac{1}{2} m(x) = T'_n(x). \quad (3.26)$$

Therefore, an appropriate distribution function $m(\xi)$ is twice the airfoil slope $T'_n(x)$ and thus the solution of each of the thin airfoil problems is

$$\phi_{ny}(x, y) = \frac{1}{\pi} \int_0^1 \frac{y T'_n(\xi)}{(x - \xi)^2 + y^2} d\xi, \quad (3.27)$$

$$\phi_{nx}(x, y) = \frac{1}{\pi} \int_0^1 \frac{(x - \xi) T'_n(\xi)}{(x - \xi)^2 + y^2} d\xi. \quad (3.28)$$

We obtain the surface values by the limit of (3.28), as y tends to zero, and using again the tangency condition to get $\phi_{ny}(x, 0)$, we obtain

$$\phi_{nx}(x, 0) = \frac{1}{\pi} \oint_0^1 \frac{T'_n(\xi)}{(x - \xi)} d\xi. \quad (3.29)$$

For the thickness-function $T(x)$, defined in (2.9), we now calculate the surface speed¹ up to the first order of τ as

$$u_{s_o}(x) = 1 + \tau \phi_{1x}(x, 0). \quad (3.30)$$

¹The indexes of u_{s_o} will become clearer in the following, here we anticipate that it stands for *surface velocity of 'outer' flow*

3 Potential flow past thin airfoil

In the present problem we find the following expression for the potential $\phi_{1x}(x, 0)$, containing logarithms of $|x|$ and $|1 - x|$ which are responsible for the singularities at $x = 0$ and $x = 1$ respectively and caused by the perturbation approach:

$$\begin{aligned} \phi_{1x}(x, 0) = & \frac{1}{2\pi(1-x+\varepsilon)^2} [\varepsilon(- (x - \varepsilon - 1)(11 + 3x(2x - 5 - 2\varepsilon) + 7\varepsilon) \\ & + 2\varepsilon(\varepsilon^2 - 1)(\ln(\varepsilon) - \ln(1 + \varepsilon))] \\ & + \frac{\ln|x| - \ln|1-x|}{\pi(1-x+\varepsilon)^2} [(x-1)(3x^3\varepsilon - 3x^2\varepsilon(3+2\varepsilon) \\ & - (1+\varepsilon)(1+\varepsilon(4+\varepsilon)) + x(1+\varepsilon)(1+\varepsilon(8+3\varepsilon))]. \end{aligned} \quad (3.31)$$

The velocity perturbation $u_{s_o}(x) - 1$ at the surface for different curvatures $k < 0$ (see Figure 3.1) shows therefore vertical tangents at $x = 1$.

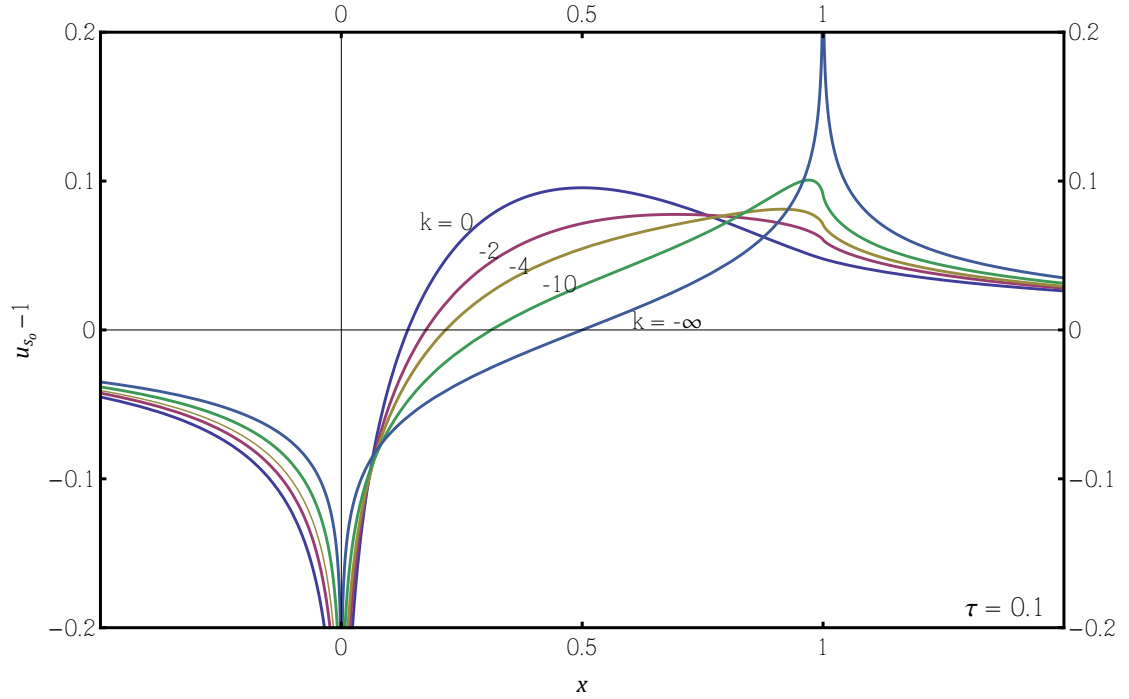


Figure 3.1: Velocity perturbation $u_{s_o}(x) - 1$ for different curvatures k at $x = 1$, $\tau = 0.1$.

3.4 Matching with a local solution near sharp edge

In this subsection we want to correct the non-uniformity (ln-singularity) in the vicinity of the leading edge by introducing a local solution and matching it with the one obtained in section 3.3. The thin airfoil solution in the present case fails within a narrow region at the leading edge, which we call *inner region* in the following. Accordingly we call the region, where the thin airfoil solution is eligible, *outer region* and use the small letters 'i' and 'o' as indexes² to distinguish between them. The existence of an *overlap region* between the inner and the outer region, according to *Kaplun's extension theorem* (see e. g. [2]), allows for matching of the two corresponding solutions (*local/inner solution* and *outer solution*) in the spirit of matched asymptotic expansions.

3.4.1 Inner variables

Studying the inner region requires appropriately magnified variables. Expansion of the velocity perturbation around the sharp edge (stagnation point) at $x = 0$, leads to

$$u_{s_o}(x) - 1 \sim \frac{\tau(2 + 8\varepsilon + 2\varepsilon^2)}{2\pi(1 + \varepsilon)} \ln|x| + \frac{\tau}{2\pi(1 + \varepsilon)} [11\varepsilon + 7\varepsilon^2 - 2\varepsilon^2 \ln(\varepsilon) + 2\varepsilon^3 \ln(\varepsilon) + 2\varepsilon^2 \ln(1 + \varepsilon) - 2\varepsilon^3 \ln(1 + \varepsilon)] + O(x) \quad (3.32)$$

as $x \rightarrow 0$ and

$$u_{s_o}(x) - 1 |_{\varepsilon=1} \sim \frac{\tau(18 + 12 \ln|x|)}{4\pi} + O(x), \quad (3.33)$$

which shows, that the perturbation velocity at the surface behaves as $\tau \ln(x)$ for $x \rightarrow 0$.

The asymptotic expansion in (3.5) is only valid if we assume every function in the sequence growing strictly slower than the preceding function. Therefore $|\tau \ln|x|| < 1$ has to hold for the validity of the solution. So $\tau \ln|x|$ is negative for $x < 1$ but at the most it is allowed to be equal to -1 .

²we will use the capitals 'I' and 'O' to distinguish between the two corresponding coordinate systems later

3 Potential flow past thin airfoil

This consideration leads to the appropriate scaling within the inner region:

$$\begin{aligned}\tau \ln(x) &= -1 \\ e^{\tau \ln(x)} &= (e^{\ln(x)})^\tau = x^\tau = e^{-1} \\ x &= \sqrt[\tau]{e^{-1}} = e^{-\frac{1}{\tau}}\end{aligned}\tag{3.34}$$

Hence, the thickness of the inner region is of the order $x \sim e^{-\frac{1}{\tau}}$ (i. e. exponentially small).

Now we can introduce *inner coordinates* x_i and y_i which are of order unity within the inner region

$$x_i = x e^{\frac{1}{\tau}}, \quad y_i = y e^{\frac{1}{\tau}}.\tag{3.35}$$

Correspondingly we call x and y *outer coordinates* in the following.

3.4.2 Inner solution

Within the narrow inner region, the sharp edge of the half-body at $x = 0$, can be approximated by a wedge (see Figure 3.2) with the slope given by

$$\tau\alpha(\varepsilon) = \tau T'(x = 0; \varepsilon) = \tau \left(3\varepsilon + \frac{(1 - \varepsilon)(1 + 2\varepsilon)}{1 + \varepsilon} \right), \quad 0 < \varepsilon < 1.\tag{3.36}$$

The description of a potential flow past a wedge can easily be found by transformation of the Laplace equation in polar coordinates (see Figure 3.3) and separation of variables or alternatively by conformal mapping. The first being the more universal method, which can be extended to three-dimensional problems, is shown in the following subsections. The method of conformal mapping can be found for example in [6].

3.4.2.1 Transformation of the Laplace equation

First, we have to transform the Laplace equation in polar coordinates through $\phi(x_i, y_i) \rightarrow \phi(r, \vartheta)$ with

$$\begin{aligned}r &:= \sqrt{x_i^2 + y_i^2}, \\ \vartheta &:= \arctan\left(\frac{y_i}{x_i}\right).\end{aligned}\tag{3.37}$$

3 Potential flow past thin airfoil

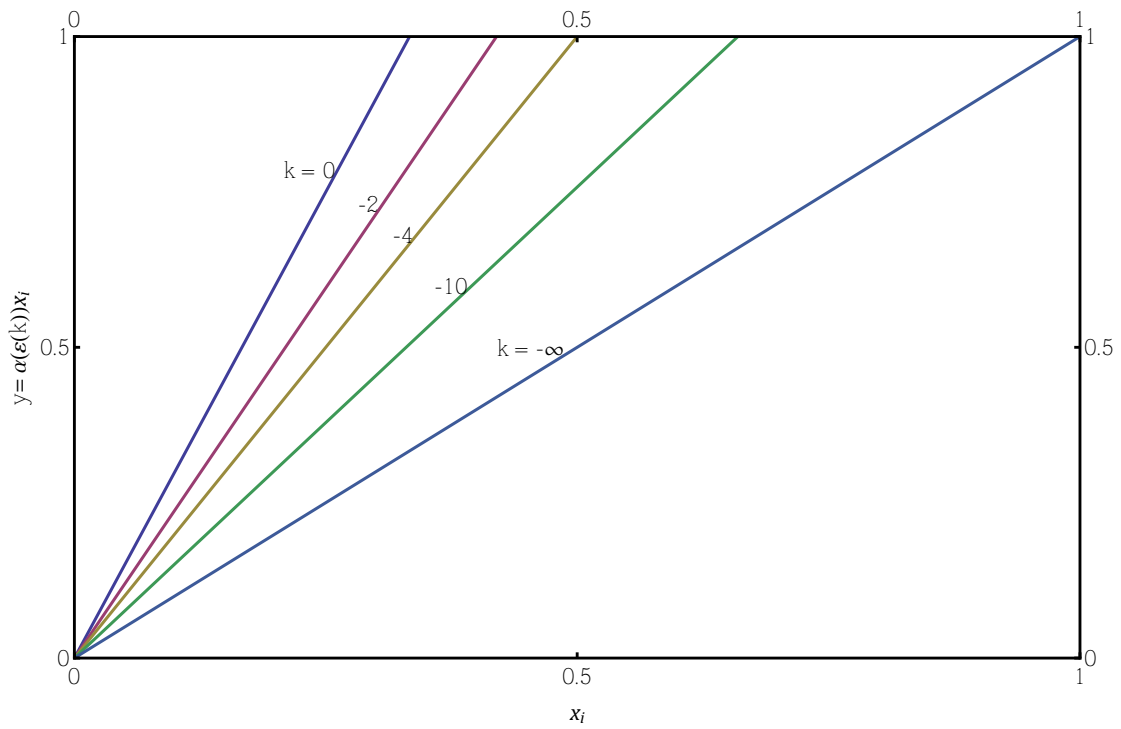


Figure 3.2: Slope of the leading edge, $\alpha(\epsilon)x_i$, for different curvatures, k , at $x = 1$.

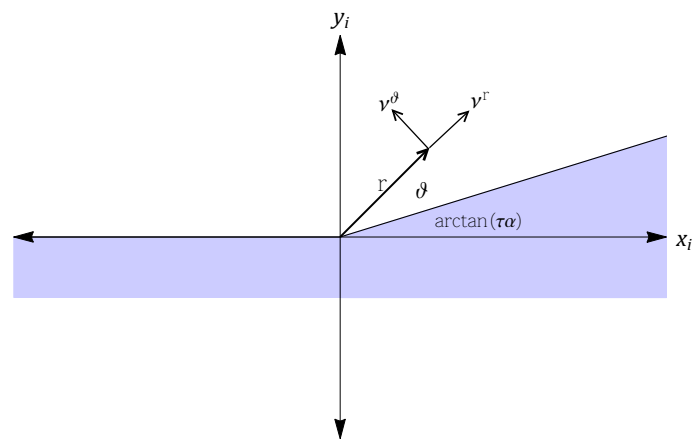


Figure 3.3: Notation in polar coordinates; v^θ , v^r -velocity components.

3 Potential flow past thin airfoil

The respective derivatives are

$$\begin{aligned}
 \phi_{x_i} &= \frac{\partial \phi}{\partial r} \frac{\partial r}{\partial x_i} + \frac{\partial \phi}{\partial \vartheta} \frac{\partial \vartheta}{\partial x_i}, \\
 \phi_{x_i x_i} &= \frac{\partial \phi_{x_i}}{\partial r} \frac{\partial r}{\partial x_i} + \frac{\partial \phi_{x_i}}{\partial \vartheta} \frac{\partial \vartheta}{\partial x_i}, \\
 \phi_{y_i} &= \frac{\partial \phi}{\partial r} \frac{\partial r}{\partial y_i} + \frac{\partial \phi}{\partial \vartheta} \frac{\partial \vartheta}{\partial y_i}, \\
 \phi_{y_i y_i} &= \frac{\partial \phi_{y_i}}{\partial r} \frac{\partial r}{\partial y_i} + \frac{\partial \phi_{y_i}}{\partial \vartheta} \frac{\partial \vartheta}{\partial y_i},
 \end{aligned} \tag{3.38}$$

where considering $x_i = r \cos \vartheta$, $y_i = r \sin \vartheta$ the partial derivatives are

$$\begin{aligned}
 \frac{\partial r}{\partial x_i} &= \frac{\partial((x_i^2 + y_i^2)^{\frac{1}{2}})}{\partial x_i} = \frac{x_i}{\sqrt{x_i^2 + y_i^2}} = \frac{r \cos \vartheta}{r} = \cos \vartheta, \\
 \frac{\partial \vartheta}{\partial x_i} &= \frac{1}{1 + \left(\frac{y_i}{x_i}\right)^2} (-y_i) \frac{1}{x_i^2} = -\frac{y_i}{x_i^2 + y_i^2} = -\frac{r \sin \vartheta}{r^2} = -\frac{\sin \vartheta}{r}, \\
 \frac{\partial \vartheta}{\partial y_i} &= \frac{1}{1 + \left(\frac{y_i}{x_i}\right)^2} \frac{1}{x_i} = \frac{x_i}{x_i^2 + y_i^2} = \frac{x_i \cos \vartheta}{r^2} = \frac{\cos \vartheta}{r}, \\
 \frac{\partial r}{\partial y_i} &= \frac{\partial((x_i^2 + y_i^2)^{\frac{1}{2}})}{\partial y_i} = \frac{y_i}{\sqrt{x_i^2 + y_i^2}} = \frac{r \sin \vartheta}{r} = \sin \vartheta.
 \end{aligned} \tag{3.39}$$

Substituting (3.38) and (3.39) into (3.2) we obtain the Laplace equation in polar coordinates as

$$\phi_{rr} + \phi_{\vartheta\vartheta} \frac{1}{r^2} + \phi_r \frac{1}{r} = 0. \tag{3.40}$$

Whereas the respective gradient in polar coordinates is defined by

$$\nabla \phi = \frac{\partial \phi}{\partial r} \vec{e}_r + \frac{1}{r} \frac{\partial \phi}{\partial \vartheta} \vec{e}_\vartheta = \nu^r \vec{e}_r + \nu^\vartheta \vec{e}_\vartheta, \tag{3.41}$$

where ν^r and ν^ϑ are the tangential and normal velocities with respect to the surface of the investigated wedge, respectively.

3 Potential flow past thin airfoil

3.4.2.2 Separation of variables

To solve (3.40) we use the ansatz:

$$\phi = R(r)\theta(\vartheta), \quad (3.42)$$

and thus the method of separation of variables. In other words, we rewrite the equation so that each of the two variables, r and ϑ , occur on a different side of the equation. Such an equation can only be satisfied, if both sides are equal to the same constant, say λ^2 . In the present case this approach results in two ordinary differential equations for the two variables, which can be easily solved separately and then combined according to (3.42).

The ansatz (3.42) inserted into (3.40) gives

$$R''\theta + \theta''R\frac{1}{r^2} + R'\theta\frac{1}{r} = 0. \quad (3.43)$$

Multiplying both sides by $r^2/(R\theta)$ to separate the variables we get

$$\frac{R''r^2}{R} + \frac{\theta''}{\theta} + \frac{R'r}{R} = 0, \quad (3.44)$$

and rearranged

$$\frac{r^2}{R}R'' + \frac{r}{R}R' = -\frac{1}{\theta}\theta''. \quad (3.45)$$

Setting both sides λ^2 we obtain the two equations for r and ϑ as

$$\lambda^2 = \frac{r^2}{R}R'' + \frac{r}{R}R' \quad \Rightarrow \quad r^2R'' + rR' - \lambda^2R = 0, \quad (3.46)$$

$$\lambda^2 = -\frac{1}{\theta}\theta'' \quad \Rightarrow \quad \theta'' + \lambda^2\theta = 0, \quad (3.47)$$

the first being an ordinary *Cauchy-Euler differential equation* and the second being an ordinary *differential equation with constant coefficients* with the solutions (see e. g. [4])

$$R(r) = C_1r^\lambda + C_2r^{-\lambda} \text{ and} \quad (3.48)$$

$$\theta(\vartheta) = D_1 \cos(\lambda\vartheta) + D_2 \sin(\lambda\vartheta), \quad (3.49)$$

where C_1, C_2, D_1 and D_2 denote integration constants.

3.4.2.3 Solution and boundary conditions

According to (3.42) the solution of (3.40) is found to be:

$$\phi(r, \vartheta) = [C_1 r^\lambda + C_2 r^{-\lambda}] [D_1 \cos(\lambda\vartheta) + D_2 \sin(\lambda\vartheta)] \quad (3.50)$$

Assuming $\lambda > 0$ and to avoid a singularity at $r = 0$, we have to set $C_2 = 0$. The problem now contains two remaining integration constants, $E_1 = C_1 D_1$ and $E_2 = C_1 D_2$, which can be found using the tangency conditions at the surface. Thus we have

$$\phi(r, \vartheta) = r^\lambda (E_1 \cos(\lambda\vartheta) + E_2 \sin(\lambda\vartheta)), \quad (3.51)$$

and the partial derivatives with respect to ϑ and r are

$$\phi_\vartheta(r, \vartheta) = r^\lambda \lambda (E_2 \cos(\lambda\vartheta) - E_1 \sin(\lambda\vartheta)), \quad (3.52)$$

$$\phi_r(r, \vartheta) = \lambda r^{\lambda-1} (E_1 \cos(\lambda\vartheta) + E_2 \sin(\lambda\vartheta)). \quad (3.53)$$

Additionally the boundary conditions for the normal component of the velocity ν^ϑ (see Figure 3.3) are

$$\nu^\vartheta(\vartheta = \pi) = \frac{1}{r} \phi_\vartheta(\vartheta = \pi) = 0 \text{ and}$$

$$\nu^\vartheta(\vartheta = \arctan(\tau\alpha)) = \frac{1}{r} \phi_\vartheta(\vartheta = \arctan(\tau\alpha)) = 0$$

and therefore

$$\lambda r^{\lambda-1} (E_2 \cos(\lambda\pi) - E_1 \sin(\lambda\pi)) = 0, \quad (3.54)$$

$$\lambda r^{\lambda-1} (E_2 \cos(\lambda \arctan(\tau\alpha)) - E_1 \sin(\lambda \arctan(\tau\alpha))) = 0. \quad (3.55)$$

Considering the two equations (3.54) and (3.55), we can calculate the separation constant λ as

$$\begin{aligned} & \frac{\cos(\lambda \arctan(\tau\alpha))}{\cos(\lambda\pi)} - \frac{\sin(\lambda \arctan(\tau\alpha))}{\sin(\lambda\pi)} = 0 \\ \implies & \sin(\lambda\pi) \cos(\lambda \arctan(\tau\alpha)) - \cos(\lambda\pi) \sin(\lambda \arctan(\tau\alpha)) = 0 \\ & \implies \sin(\lambda(\pi - \arctan(\tau\alpha))) = 0 \quad (3.56) \\ \implies & \lambda(\pi - \arctan(\tau\alpha)) = j\pi, \quad j = 1, 2, \dots \end{aligned}$$

$$\implies \lambda_j = \frac{j\pi}{\pi - \arctan(\tau\alpha)}.$$

3 Potential flow past thin airfoil

Thus, we obtain the solution as a sum over all integers j by

$$\phi(r, \vartheta) = \sum_{j=1}^{\infty} r^{\lambda_j} (E_1 \cos(\lambda_j \vartheta) + E_2 \sin(\lambda_j \vartheta)). \quad (3.57)$$

Considering the immediate neighborhood of the stagnation point, where $r \ll 1$, we will only preserve the first term of (3.57).

Now we can define one of the constants E_1 and E_2 by using again (3.54),(3.55), and the abbreviation $\beta := \arctan(\tau\alpha)$ as

$$E_2 = E_1 \frac{\sin(\lambda\pi)}{\cos(\lambda\pi)} = E_1 \frac{\sin(\lambda\beta)}{\cos(\lambda\beta)}, \quad (3.58)$$

and obtain the surface speed at $\vartheta = \pi$ and $\vartheta = \beta$ by

$$\begin{aligned} \nu^r(r, \vartheta = \pi) &= \lambda r^{\lambda-1} E_1 \left[\cos(\lambda\pi) + \frac{\sin(\lambda\pi)}{\cos(\lambda\pi)} \sin(\lambda\pi) \right] = \lambda r^{\lambda-1} E_1 \frac{1}{\cos(\lambda\pi)}, \\ \nu^r(r, \vartheta = \beta) &= \lambda r^{\lambda-1} E_1 \left[\cos(\lambda\beta) + \frac{\sin(\lambda\pi)}{\cos(\lambda\pi)} \sin(\lambda\beta) \right] = \lambda r^{\lambda-1} E_1 \underbrace{\frac{1}{\cos(\lambda\pi)}}_{:=U_i}. \end{aligned} \quad (3.59)$$

The result contains still an unknown constant U_i , which has to be found by matching this inner solution with the outer solution. For a small angle β and small y we can approximate

$$\lambda = \frac{\pi}{\pi - \beta} \sim 1 \text{ and } r \sim x_i. \quad (3.60)$$

Consequently, the inner solution for the surface speed is described by

$$u_{s_i} \sim U_i x_i^{\frac{\arctan(\tau\alpha(\varepsilon))}{\pi - \arctan(\tau\alpha(\varepsilon))}}, \quad (3.61)$$

where U_i can be interpreted as the free-stream speed at $x_i = 1$ (see [10]). The fact that this solution diverges at infinity, is not a problem since this solution is only used within the inner region close to $x = 0$.

3.4.3 Van Dyke's matching rule

Van Dyke's matching rule adjusted to the present problem is formulated in (3.62). The indexes I and O denote for inner and outer coordinates, whereas m and n indicate the number of terms to be considered. Detailed instruction about the usage of this and other matching procedures including a discussion of their respective scope can be found in [8]. According to the matching rule

$$[f_O^n]^m = [f_I^m]^n, \quad (3.62)$$

3 Potential flow past thin airfoil

we need to equate the n -term outer solution f_O^n rewritten in inner coordinates $[f_O^n]_I$ and expanded in Taylor series up to the m th-term $[f_O^n]^m$ to the m -term inner solution f_I^m rewritten in outer coordinates $[f_I^m]_O$ expanded in Taylor series up to the n th-term $[f_I^m]^n$. The matching procedure usually follows a step by step scheme starting with $n = 1, m = 1$ and then checking possible secondary effects by setting $n = 2, m = 1$ before proceeding with $n = 2, m = 2$ and so on. In this case, (3.61) shows the approximation of the inner solution to any order, because it was not obtained by an asymptotic expansion. Hence, we can treat any desired approximation at once. In (3.3), we calculated the surface speed up to the first order of τ , which represents a 2-term outer solution (see (3.31)). For $n = 2, m = 2$ the matching steps are presented in the following:

- 2-term outer solution in outer coordinates

$$\begin{aligned}
 u_{s_oO}^2 \sim 1 + \tau & \left(\frac{1}{2\pi(1-x+\varepsilon)^2} [\varepsilon ((1-x+\varepsilon) (11 + 3x (2x \right. \\
 & - 5 - 2\varepsilon) + 7\varepsilon) + 2\varepsilon (\varepsilon^2 - 1) (\ln(\varepsilon) - \ln(1+\varepsilon))] \\
 & + \frac{\ln|x| - \ln|1-x|}{\pi(1-x+\varepsilon)^2} [(x-1) (3x^3\varepsilon - 3x^2\varepsilon (3+2\varepsilon) \\
 & \left. - (1+\varepsilon) (1+\varepsilon(4+\varepsilon)) + x(1+\varepsilon) (1+\varepsilon(8+3\varepsilon)))] \right), \tag{3.63}
 \end{aligned}$$

- rewritten in inner coordinates:

$$\begin{aligned}
 [u_{s_oO}^2]_I \sim 1 + \tau & \left(\frac{1}{2\pi(1-e^{-1/\tau}x_i+\varepsilon)^2} [\varepsilon ((1-e^{-1/\tau}x_i+\varepsilon) (11 \right. \\
 & + 3e^{-1/\tau}x_i (2e^{-1/\tau}x_i - 5 - 2\varepsilon) + 7\varepsilon) + 2\varepsilon (\varepsilon^2 \\
 & - 1) (\ln(\varepsilon) - \ln(1+\varepsilon))] \\
 & + \frac{\ln(e^{-1/\tau}|x|) - \ln|1-e^{-1/\tau}x_i|}{\pi(1-e^{-1/\tau}x_i+\varepsilon)^2} [(e^{-1/\tau}x_i-1) (3e^{-3/\tau}x_i^3\varepsilon \\
 & - 3e^{-2/\tau}x_i^2\varepsilon (3+2\varepsilon) - (1+\varepsilon) (1+\varepsilon(4+\varepsilon)) \\
 & \left. + e^{-1/\tau}x_i (1+\varepsilon) (1+\varepsilon(8+3\varepsilon)))] \right), \tag{3.64}
 \end{aligned}$$

3 Potential flow past thin airfoil

- expanded in Taylor series and truncated after the 2nd term (first order of τ):

$$\begin{aligned} [u_{s_o}^2]_I^2 &\sim \left(1 - \frac{2 + 8\varepsilon + 2\varepsilon^2}{2\pi(1 + \varepsilon)}\right) \\ &+ \frac{\tau}{2\pi(1 + \varepsilon)} [2(1 + \varepsilon(4 + \varepsilon)) \ln |x_i| + \varepsilon(11 + 7\varepsilon \\ &+ 2(\varepsilon - 1)\varepsilon(\ln(\varepsilon) - \ln(1 + \varepsilon)))], \end{aligned} \quad (3.65)$$

... once more we need to rewrite this result in outer coordinates because the final comparison of the two results according to (3.62) can only be done in one coordinate system! Thus we find:

$$\begin{aligned} \left[[u_{s_o}^2]_I^2 \right]_O &\sim 1 + \frac{\tau}{2\pi(1 + \varepsilon)} [2(1 + \varepsilon(4 + \varepsilon)) \ln |x| + \varepsilon(11 + 7\varepsilon) \\ &+ 2(\varepsilon - 1)\varepsilon^2(\ln(\varepsilon) - \ln(1 + \varepsilon))], \end{aligned} \quad (3.66)$$

- inner solution in inner coordinates:

$$u_{s_i}^2 \sim U_i x_i^{\frac{\arctan\left(\tau\left(3\varepsilon\frac{(1-\varepsilon)(1+2\varepsilon)}{1+\varepsilon}\right)\right)}{\pi - \arctan\left(\tau\left(3\varepsilon\frac{(1-\varepsilon)(1+2\varepsilon)}{1+\varepsilon}\right)\right)}}, \quad (3.67)$$

- rewritten in outer coordinates:

$$[u_{s_i}^2]_O \sim U_i (e^{1/\tau} x)^{\frac{\arctan\left(\tau\left(3\varepsilon\frac{(1-\varepsilon)(1+2\varepsilon)}{1+\varepsilon}\right)\right)}{\pi - \arctan\left(\tau\left(3\varepsilon\frac{(1-\varepsilon)(1+2\varepsilon)}{1+\varepsilon}\right)\right)}}, \quad (3.68)$$

- expanded in Taylor series and truncated after the 2nd term (first order of τ):

$$[u_{s_i}^2]_O^2 \sim U_i e^{\frac{1+4\varepsilon+\varepsilon^2}{\pi+\pi\varepsilon}} \left(1 + \tau \frac{(1 + 4\varepsilon + \varepsilon^2)^2 + (\pi(1 + \varepsilon)(1 + 4\varepsilon + \varepsilon^2)) \ln |x|}{\pi^2(1 + \varepsilon)^2}\right). \quad (3.69)$$

Now we need to equate (3.66) and (3.69) to obtain the unknown constant U_i (up to the first order of τ , because we only matched with $n = 2$, $m = 2$ and therefore

3 Potential flow past thin airfoil

in higher order, U_i still contains the outer variable x):

$$\begin{aligned}
U_i &\sim e^{-\frac{1+4\varepsilon+\varepsilon^2}{\pi+\pi\varepsilon}} \left(1 + \frac{\tau}{2\pi(1+\varepsilon)} [\varepsilon(11+7\varepsilon) + 2(1+\varepsilon(4+\varepsilon)) \ln|x| \right. \\
&\quad \left. + 2(\varepsilon-1)\varepsilon^2(\ln(\varepsilon) - \ln(1+\varepsilon))] \right) \left(1 - \frac{\tau}{\pi^2(1+\varepsilon)^2} [(1 \right. \\
&\quad \left. + 4\varepsilon + \varepsilon^2)^2 + (\pi(1+\varepsilon)(1+4\varepsilon+\varepsilon^2)) \ln|x|] \right) \\
&\sim e^{-\frac{1+4\varepsilon+\varepsilon^2}{\pi+\pi\varepsilon}} \left(1 + \frac{\tau}{2\pi^2(1+\varepsilon)^2} [\varepsilon(\pi(1+\varepsilon)(11+7\varepsilon) - 2(4+\varepsilon)(2+\varepsilon(4+\varepsilon))) \right. \\
&\quad \left. + 2\pi\varepsilon^2(\varepsilon^2-1)(\ln(\varepsilon) - \ln(1+\varepsilon)) - 2] \right) + O(\tau^2).
\end{aligned} \tag{3.70}$$

3.5 Compound solution

At this point the inner and the outer solution are both determined. However, for a numerical evaluation of the obtained functions, as required for the investigation of the boundary layer in the following, we need to combine them into a composite approximation (*compound solution*) of the surface speed, which is uniformly valid in the whole x -range $[0, 1]$ of the half-body. This is possible, if we assume that the ranges of validity of the outer and inner solution overlap in an intermediate range according to Kaplun's extension theorem, where both solutions tend to the same function for $\tau \rightarrow 0$ (*overlap region*).

There are several methods to obtain a compound solution, which cannot be considered to be distinct. Nevertheless each such uniformly valid solution, no matter how it was obtained, must be equivalent to the inner solution within the inner region and to the outer solution within the outer region. Widely used are the multiplicative and the additive method (see e.g. [8]). Using the notation explained in 3.4.3 we can formulate them by

$$\text{additive method: } f^{(n,m)} = f_O^n + f_I^m - [f_I^m]_O^n, \tag{3.71}$$

$$\text{multiplicative method: } f^{(n,m)} = \frac{f_O^n f_I^m}{[f_I^m]_O^n} \tag{3.72}$$

3 Potential flow past thin airfoil

where $[f_I^m]^n$ represents the common part of the outer and inner solution (in the overlap region).

Both can be justified expanding the right hand side with fixed outer coordinates reproducing the outer solution and similarly using (3.62) with fixed inner coordinates reproducing the inner solution except of higher order terms (h.o.t.). Doing so, we get

$$\text{additive method: } f_O^n + [f_I^m]^n + h.o.t. - [f_I^m]^n = f_O^n + h.o.t., \quad (3.73)$$

$$[f_O^n]^m + h.o.t. + f_I^m - [f_I^m]^n = f_I^m + h.o.t.,$$

$$\text{multiplicative method: } \frac{f_O^n ([f_I^m]^n + h.o.t.)}{[f_I^m]^n} = f_O^n, \quad (3.74)$$

$$\frac{([f_O^n]^m + h.o.t.) f_I^m}{[f_I^m]^n} = f_I^m.$$

In some cases both of the methods can lead to an incorrect solution (see [8]). We have to assure that the higher order terms in (3.73) and (3.74), which we neglect, would not become infinite and thus crucial for any value of the independent variable. Furthermore, the multiplicative method cannot be used, if the common part of the solutions shows a root for one or more values of the independent variable, because in that case the higher order terms cannot be neglected and thus the common part does not cancel out of the equation (3.74). Obviously, in this situation, we would not obtain f_I^m and f_O^n , respectively. Moreover, the zero in the denominator would result in a singularity.

In the present case the logarithm in the common part of the solutions causes the multiplicative method to be inappropriate in the sense outlined above and therefore we have to use the additive method (3.71) to formulate the compound solution. We need to sum up (3.63) and (3.68) and subtract the common part stated in (3.69) after substituting U_i according to (3.70). Here we have to keep in mind, that we formulate a first order approximation ($O(\tau)$) and so we have to leave out higher order terms arriving from substituting U_i in (3.69), which is also indicated by the n in the common part $[f_I^m]^n$.

3 Potential flow past thin airfoil

Here the compound solution $u_s^{(n,m)}$ with $n = 2$ and $m = 2$ is found to be:

$$\begin{aligned}
u_s^{(2,2)}(x) = & 1 + e^{-\frac{1+4\varepsilon+\varepsilon^2}{\pi+\pi\varepsilon}} \left(e^{\frac{1}{\tau}x} \frac{\arctan\left(\tau\left(3\varepsilon\frac{(1-\varepsilon)(1+2\varepsilon)}{1+\varepsilon}\right)\right)}{\pi - \arctan\left(\tau\left(3\varepsilon\frac{(1-\varepsilon)(1+2\varepsilon)}{1+\varepsilon}\right)\right)} \right) \left(1 \right. \\
& + \frac{\tau}{2\pi^2(1+\varepsilon)^2} \left[\varepsilon(\pi(1+\varepsilon)(11+7\varepsilon) - 2(4+\varepsilon)(2+\varepsilon(4+\varepsilon))) \right. \\
& \left. \left. + 2\pi\varepsilon^2(\varepsilon^2 - 1)(\ln(\varepsilon) - \ln(1+\varepsilon)) - 2 \right] \right) \\
& - \frac{\ln|1-x|}{(\pi(1+\varepsilon)(1-x+\varepsilon)^2)} \left[\tau(x-1)(1+\varepsilon) (3x^3\varepsilon - 3x^2\varepsilon(3+2\varepsilon) \right. \\
& \left. - (1+\varepsilon)(1+\varepsilon(4+\varepsilon)) + x(1+\varepsilon)(1+\varepsilon(8+3\varepsilon))) \right] \quad (3.75) \\
& + \frac{x \ln|x|}{(\pi(1+\varepsilon)(1-x+\varepsilon)^2)} \left[\tau\varepsilon (3x^3(1+\varepsilon) - 6x^2(1+\varepsilon)(2+\varepsilon) \right. \\
& \left. - 2(1+\varepsilon)(3+\varepsilon)(1+2\varepsilon) + x(5+3\varepsilon)(3+\varepsilon(5+\varepsilon))) \right] \\
& - \frac{1}{(\pi(1+\varepsilon)(1-x+\varepsilon)^2)} \left[\pi(1+\varepsilon)(1-x+\varepsilon)^2 + x (x \right. \\
& \left. - \varepsilon - 1) \varepsilon(3x(1+\varepsilon) - (2+\varepsilon)(1+3\varepsilon))\tau + x(\varepsilon - 1)\varepsilon^2 (x \right. \\
& \left. - 2(1+\varepsilon)) \tau (\ln(\varepsilon) - \ln(1+\varepsilon)) \right].
\end{aligned}$$

Evidently the singularity at the leading edge disappeared, compared to (3.63). All terms containing $\ln|x|$ are multiplied by some power of x bigger than one and $\lim_{x \rightarrow 0} u_s^{(2,2)}(x) = 0$ (see Figure 3.4)³, which we can see even clearer setting $\varepsilon = 1$ or $k = 0$, whereby we obtain the simpler expression

³Note, that throughout this chapter a uniform color code is used for different k to facilitate comparison of the various solutions. A new independent color code will be used in chapter 4 for the presentation of the boundary layer behavior.

3 Potential flow past thin airfoil

$$u_s^{(2,2)}(x) \Big|_{\varepsilon=1} = U \left(e^{-3/\pi} (e^{1/\tau} x)^{\frac{\arctan(3\tau)}{\pi - \arctan(3\tau)}} \left(1 + \frac{(-72 + 36\pi)\tau}{8\pi^2} \right) - \frac{\tau(3x - 3(x-1)^2 \ln|1-x| + 3(x-2)x \ln|x|)}{\pi} \right). \quad (3.76)$$

Furthermore, with $\varepsilon \rightarrow 0$ or $k \rightarrow -\infty$ we get

$$u_s^{(2,2)}(x) \Big|_{\varepsilon \rightarrow 0} = \frac{e^{-\frac{\pi\tau + (\pi + \tau)\arctan(\tau)}{\pi\tau(\pi - \arctan(\tau))}} x^{\frac{\arctan(\tau)}{\pi - \arctan(\tau)}} (\pi^2 - \tau) - \pi\tau \ln|x-1|}{\pi^2}. \quad (3.77)$$

Whereas the presented compound solution is very accurate within the inner region

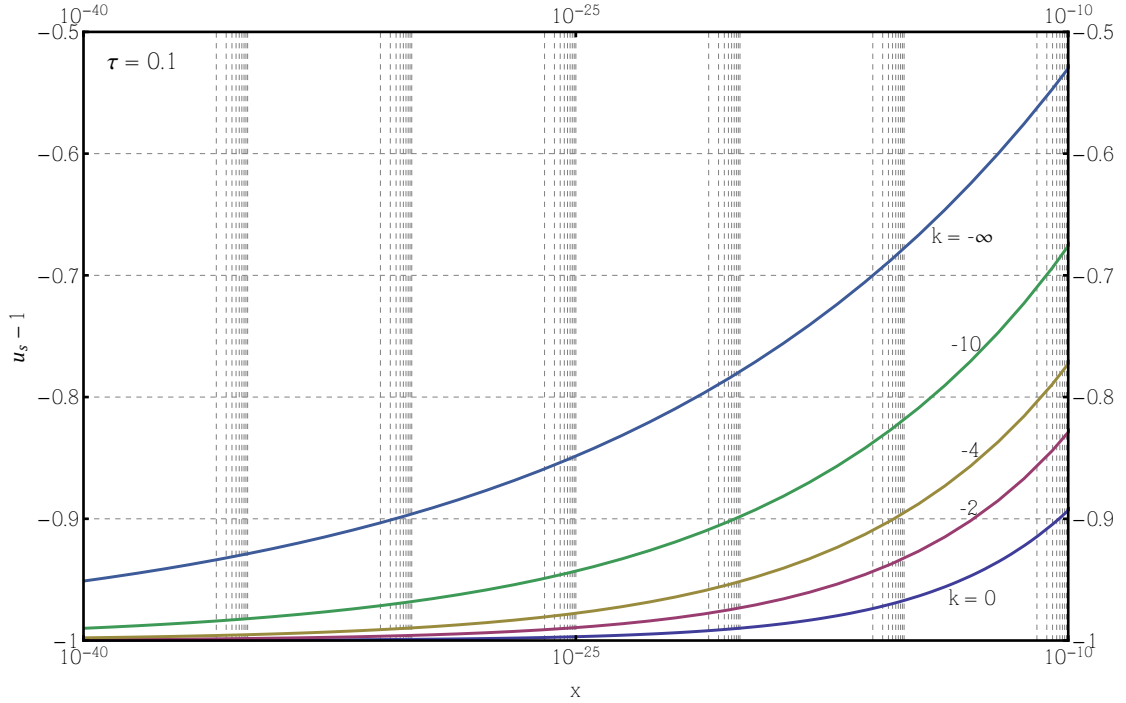


Figure 3.4: Velocity perturbation, compound solution $\lim_{x \rightarrow 0} (u_s(x) - 1) = -1$, $\tau = 0.1$.

(see Figure 3.5), in outer region the accuracy is a bit lower improving as $k \rightarrow -\infty$. This may be due to the fact that we approximated the sharp edge at $x = 0$ with the slope of the tangent at that point, $\tau T'(0, \varepsilon)$, and in the limit of $k \rightarrow -\infty$ the ramp function $T(x)$ degenerates to a linear function showing exactly the assumed slope. However, it can be seen in Figure 3.6 that the inaccuracy does not exceed

3 Potential flow past thin airfoil

the magnitude of τ , which means that up to the first order of τ , the approximation is satisfactory also for the outer region. Moreover Figures 3.7(a) and 3.7(b) are showing the dependence of the accuracy of the compound solution on the thickness parameter τ . It increases as $\tau \rightarrow 0$.

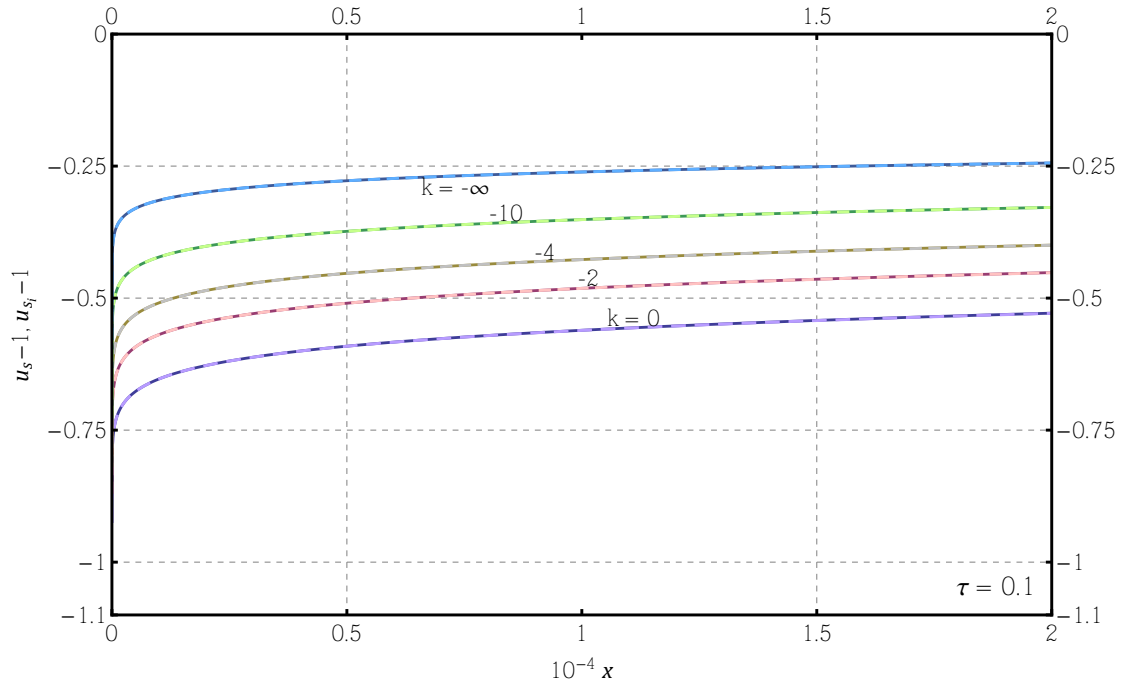


Figure 3.5: Velocity perturbation, compound solution (solid line) compared to the inner solution (dashed line), $\tau = 0.1$.

3 Potential flow past thin airfoil

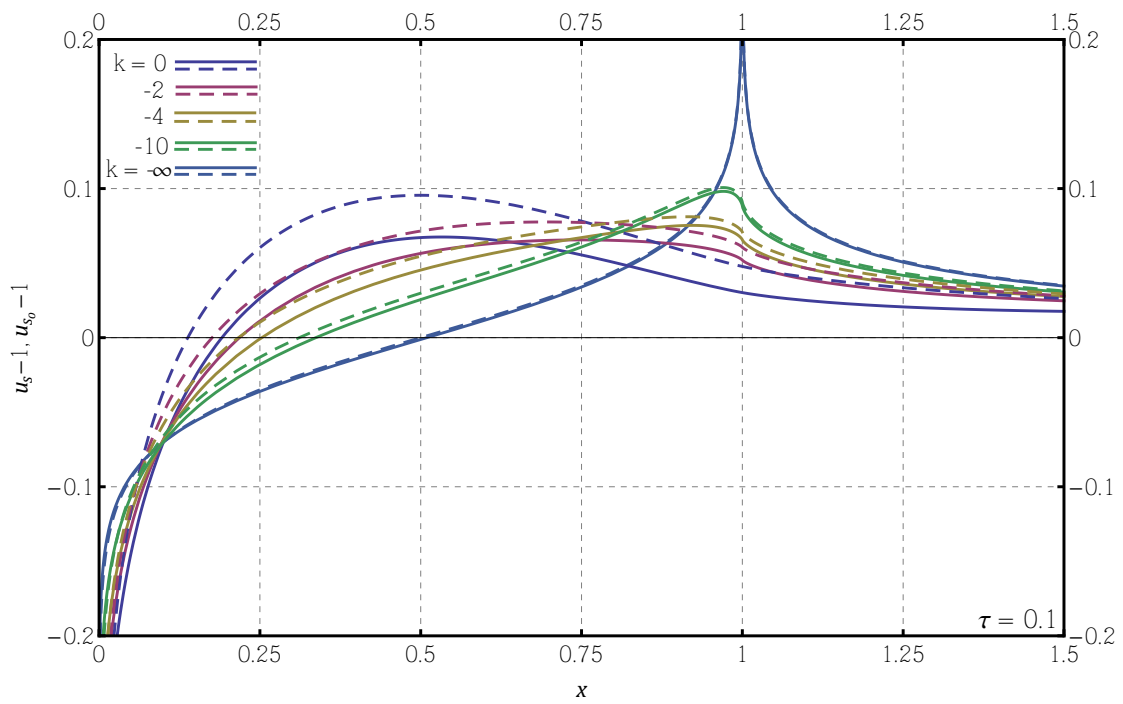
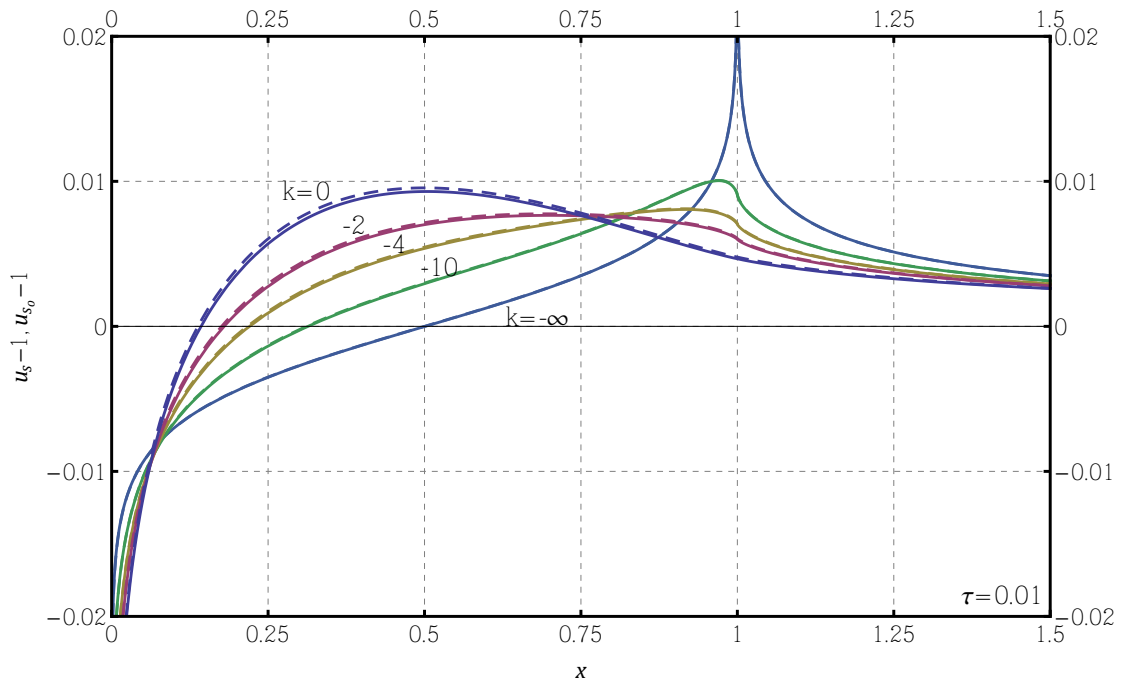
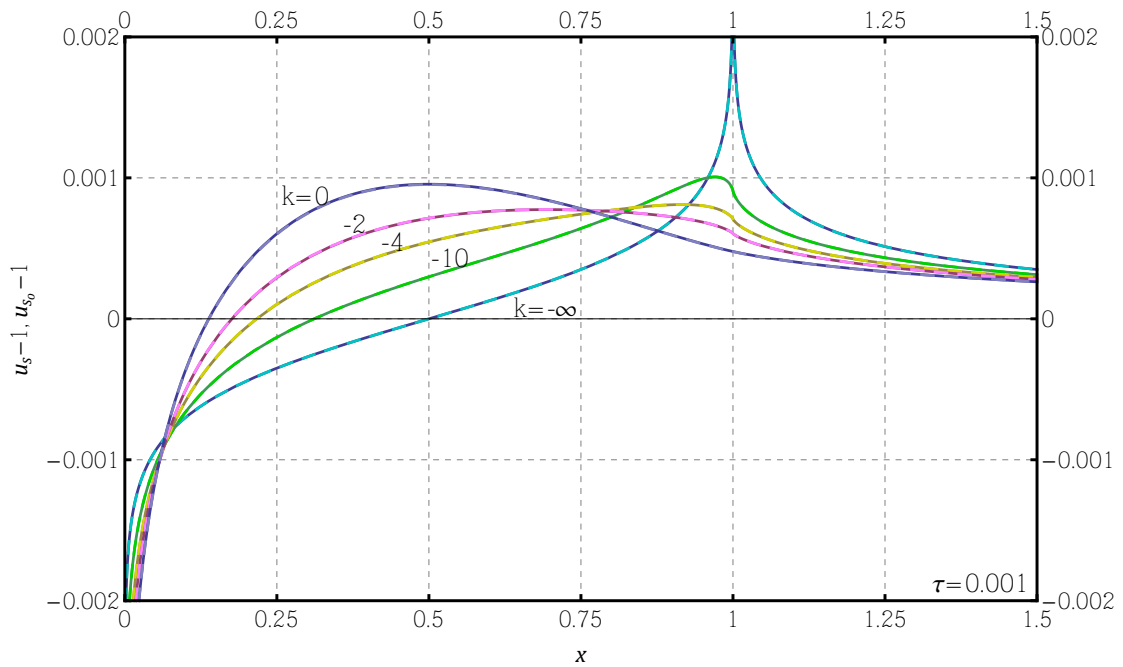


Figure 3.6: Velocity perturbation, compound solution (solid line) compared to the outer solution (dashed line), $\tau = 0.1$.

3 Potential flow past thin airfoil



(a) $\tau = 0.01$, compound solution (solid line) compared to the outer solution (dashed line)



(b) $\tau = 0.001$, compound solution (solid line) compared to the outer solution (dashed line)

Figure 3.7: Improving accuracy of the compound solution with decreasing thickness parameter τ .

4 Behavior of the boundary layer

4.1 First order boundary layer theory

Until now, we assumed a potential flow to find an approximation for the velocity distribution along the given family of half-bodies. In vicinity of the boundaries of a flow field, such as solid walls, this approximation is not longer valid. This is due to the no-slip condition at the wall which causes high velocity gradients normal to the wall $\partial u/\partial y$. On the other hand in some distance of the wall, depending on the Reynolds number, the velocity distribution has to match with the external flow, which is only slightly different to the undisturbed oncoming flow (we obtained the results by asymptotic expansion assuming very small disturbances in chapter 3).

The area between the solid surface of the half-body and the surrounding, approximately frictionless flow is called *boundary layer* and the concept to divide a flow field into these two regions to account for friction only in the immediate neighborhood of a solid wall or, more generally, of an interface between two different flow fields¹ was first introduced by *Ludwig Prandtl* in 1904 and led to a significant simplification of the governing equations. This is possible due to an estimate of the magnitude of each term of the Navier-Stokes equations, assuming very large Reynolds numbers, which allows for dropping terms which are considered small compared to others. A short description of the derivation of the partial differential equation, which was finally solved numerically, is shown in section 4.2 for a better understanding of the whole strategy and a justification for the application of this theory. A more detailed presentation of the whole theory (including the second order) can be found in [3] or [7].

4.2 Derivation of the Prandtl equation

We start with the dimensionless Navier-Stokes equations for a steady flow, shown in (2.4a) to (2.4b), using a coordinate system, where the x -axis is parallel to the

¹Such an interface occurs for example also between two frictionless flow fields with different velocities. [3]

4 Behavior of the boundary layer

oncoming flow and the y -axis is perpendicular to the surface. Hence, we have a nonlinear system of equations for the three unknown functions $u_b = u_b(x, y)$, $v_b = v_b(x, y)$, and $p = p(x, y)$, which are

$$\text{Continuity equation:} \quad \frac{\partial u_b}{\partial x} + \frac{\partial v_b}{\partial y} = 0, \quad (4.1a)$$

Equation of motion:

$$x\text{-direction:} \quad u_b \frac{\partial u_b}{\partial x} + v_b \frac{\partial u_b}{\partial y} = -\frac{\partial p}{\partial x} + \frac{1}{Re} \left(\frac{\partial^2 u_b}{\partial x^2} + \frac{\partial^2 u_b}{\partial y^2} \right), \quad (4.1b)$$

$$y\text{-direction:} \quad u_b \frac{\partial v_b}{\partial x} + v_b \frac{\partial v_b}{\partial y} = -\frac{\partial p}{\partial y} + \frac{1}{Re} \left(\frac{\partial^2 v_b}{\partial x^2} + \frac{\partial^2 v_b}{\partial y^2} \right), \quad (4.1c)$$

where the index 'b' is used to distinguish between the velocity field and components within the potential flow and the boundary layer.

The equations of motion show the singular character of this theory. In case of $Re \rightarrow \infty$, the terms containing the second derivative of the velocity tend to zero and thus we should choose an asymptotic expansion as an ansatz for the quantities similar to the thin airfoil expansion in section 3.2 with an appropriate perturbation parameter. However, in the present study we consider only the first order, which means, that we just need to 'scale the normal coordinate' to account for the slenderness of the boundary layer. Thus, we have to make an estimate of the thickness of the boundary layer, which we denote with Δ . Considering the continuity equation (4.1a) we can conclude that, if $\partial u_b / \partial x$ is of order unity and y of order $O(\Delta)$, also v_b is of $O(\Delta)$. If we want to account for friction in the boundary layer, the viscous forces must be of the same order as the inertia forces. Due to (4.1b), this only holds if $\Delta \sim 1/\sqrt{Re}$, because all terms on the left as well as $\partial p / \partial x$ are of order unity. Consequently, the quantities in the normal direction have to be scaled accordingly, which we do by setting

$$\bar{y} = y\sqrt{Re} \quad \text{and} \quad \bar{v}_b = v_b\sqrt{Re}. \quad (4.2)$$

Still accounting for the order of magnitude of the terms, we can see that the viscous term in x -direction in (4.1b) can be neglected with respect to one in y -direction. Integrating equation (4.1c) with respect to y reveals, that the pressure increase p across the thin layer is of order $O(\Delta^2)$. Hence, in leading order it is negligible and we can therefore assume that the pressure doesn't change in this direction. It remains nearly the same from the outer edge of the boundary layer, where it must match with the pressure of the external potential flow, down to the surface and must therefore be defined through (3.76). Obviously (4.1b) at the interface to the

4 Behavior of the boundary layer

potential flow, where viscous forces are neglected and the tangential condition is satisfied, becomes

$$u_s \frac{\partial u_s}{\partial x} = -\frac{\partial p}{\partial x}, \quad (4.3)$$

which in integrated form corresponds to the Bernoulli equation, shown in (2.8). If we consider $p(x)$ to be a known function in the sense outlined above, it means that a third equation is not needed any more and that the system of three equations (4.1a) to (4.1c) reduces to a system of just two equations for u_b and \bar{v}_b . Moreover, we changed the type of the equation in x -direction, (4.1b), to parabolic by dropping one viscous term, which is very convenient for a numerical evaluation.

The remaining system of equations to be solved, using the scaled coordinates, is therefore (*Prandtl equation*)

$$\text{Continuity equation:} \quad \frac{\partial u_b}{\partial x} + \frac{\partial \bar{v}_b}{\partial \bar{y}} = 0, \quad (4.4a)$$

$$\text{Equation of motion in } x\text{-direction:} \quad u_b \frac{\partial u_b}{\partial x} + \bar{v}_b \frac{\partial u_b}{\partial \bar{y}} = -\frac{\partial p}{\partial x} + \frac{\partial^2 u_b}{\partial \bar{y}^2}, \quad (4.4b)$$

whereby we have to keep in mind that $\partial p / \partial \bar{y} = 0$ (equation of motion in y -direction).

Now we introduce the dimensionless *stream-function* ψ , scaled with $\sqrt{Re}/\tilde{L}\tilde{U}_\infty$, which satisfies the continuity equation identically due to its definition by

$$\frac{\partial \psi}{\partial x} = -\bar{v}_b \quad \text{and} \quad \frac{\partial \psi}{\partial \bar{y}} = u_b. \quad (4.5)$$

Out of (4.4a) and (4.4b) using ψ we obtain²

$$u_b u_{bx} + \bar{v}_b u_{b\bar{y}} = u_s u_{sx} + u_b \bar{v}_{b\bar{y}}. \quad (4.6)$$

The last step is to bring the scaling function of the thickness-growth of the boundary layer, $\delta(x)$, into this equation by defining a new variable in y -direction representing a 'pseudo-similarity'³ variable $\eta = \bar{y}/\delta(x)$ and setting

$$\psi = u_s(x)\delta(x)f(x, \eta). \quad (4.7)$$

²please note that to improve readability now the lower indexes ' x ' and ' y ' (and in the following also ' η ') indicate the direction of the respective derivative

³'pseudo' because $f(x, \eta) \neq f(\eta)$, see also [1]

4 Behavior of the boundary layer

Finally, using the product rule to obtain the respective derivatives, we obtain a parabolic (in the stream-wise direction) partial differential equation to be solved for the boundary layer,

$$f_{\eta\eta\eta} + (u_s\delta\delta_x + u_{sx}\delta^2)ff_{\eta\eta} + u_{sx}\delta^2(1 - f_\eta^2) + u_s\delta^2(f_x f_{\eta\eta} - f_\eta f_{x\eta}) = 0, \quad (4.8)$$

with the boundary conditions

$$\eta = 0: f = f_\eta = 0, \quad \eta \rightarrow \infty: f_\eta \rightarrow 1. \quad (4.9)$$

From setting $(u_s\delta\delta_x + u_{sx}\delta^2) = 1$ in (4.8) we get

$$\delta(x) = \frac{1}{u_s(x)} \sqrt{2 \int_0^x u_s(s) ds}, \quad (4.10)$$

as a definition of the scaling function $\delta(x)$.

Thus we can define the quantities of interest, the wall shear stress and the displacement thickness, which are characteristic for the investigated boundary layer as

$$\sigma(x) = \frac{u_s(x)}{\delta(x)} f_{\eta\eta}(x, 0), \quad (4.11)$$

and

$$\delta^*(x) = \int_0^\infty \left(1 - \frac{u_b(x, \bar{y})}{u_s(x)} \right) d\bar{y} = \delta(x) \lim_{\eta \rightarrow \infty} (\eta - f). \quad (4.12)$$

4.2.1 Falkner-Skan equation

Solving the boundary layer equation numerically, requires beside the boundary conditions also an initial condition. In the present case such an initial condition represents the solution of the *Falkner-Skan equation*, which is a *similar solution* and one of the very few, known exact solutions of the boundary layer equation. A short discussion of its derivation is presented in this subsection to justify its suitability.

A similar solution requires $f(x, \eta) \equiv f(\eta)$, with η as the similarity variable. Thus, to find such a solution we need to transfer the partial differential equation given in (4.8) into an ordinary differential equation. This is achieved if we assume, that

$$u_{sx}\delta^2 = \beta, \quad (4.13)$$

where β is a constant, because only in this case there exist solutions, $f(\eta)$, which are independent of x and which therefore cause the terms containing mixed partial

4 Behavior of the boundary layer

derivatives of f to disappear. Considering (4.13) and (4.10) in (4.8) we obtain the Falkner-Skan equation

$$f_{\eta\eta\eta} + ff_{\eta\eta} + \beta(1 - f_\eta^2) = 0, \quad (4.14)$$

which was first deduced by V. M. Falkner and S. W. Skan (see [7]).

A suitable potential flow, which satisfies the assumption (4.13) is obtained if the velocity can be expressed through a power-law as

$$u_s = ax^m, \quad (4.15)$$

where a and m are constant. It can be found in the neighborhood of the stagnation point on a wedge with the aperture angle $\beta\pi$, where

$$\beta = \frac{2m}{m+1}. \quad (4.16)$$

One can easily proof it using the definition of δ in (4.10). Thus, in the present case, as for the approximation of the sharp leading edge we used a wedge with the aperture angle, $\arctan(\alpha(\tau\varepsilon))$, we have to set $\beta = \arctan(\alpha(\tau\varepsilon))/\pi$ to obtain an appropriate initial condition solving (4.14) in the first step of the algorithm. Moreover, we can estimate the initial value of the wall shear stress at $x = 0$ by using the approximation outlined. Substituting (4.15) into (4.10) and (4.11) we obtain

$$\delta_{FS}(x) = x^{\frac{1-m}{2}} \sqrt{\frac{2}{a(m+1)}}, \quad (4.17)$$

and

$$\sigma_{FS}(x) = x^{\frac{3m-1}{2}} \sqrt{\frac{1+m}{2}} a^3, \quad (4.18)$$

for the scaling function and the wall shear stress, respectively. Obviously as x tends to zero the wall shear stress tends to infinity for all $m < \frac{1}{3}$.

Particular cases of the solution of the Falkner-Skan equation are found by setting $\beta = 1$ ($m = 1$) or $\beta = 0$ ($m = 0$), the former representing a two-dimensional stagnation flow, the latter describing a flow along a flat plate where the corresponding equation is the well known *Blasius equation*

$$f_{\eta\eta\eta} + ff_{\eta\eta} = 0. \quad (4.19)$$

For the flat plate the displacement thickness is found to be

$$\delta_p^*(x) = \delta(x) \int_0^\infty (1 - f_\eta) d\eta = \sqrt{2x} \lim_{\eta \rightarrow \infty} (\eta - f). \quad (4.20)$$

4.3 Numerical solution of the Prandtl equation

Simplifying the Navier-Stokes equations, we have obtained the less complicated equation (4.8) in the previous section. Nevertheless, the non-linearity of the original system of equations has been preserved, which excludes the possibility of an analytical solution due to the complexity of the potential solution in the present case. In fact the Prandtl equation can be solved analytically only for very few specific examples including e. g. the flow along a flat plate or a semi-infinite wedge (with the corresponding equations (4.19) and (4.14), respectively). The favorable type of the Prandtl equation, however, makes it easy to solve it numerically, because a parabolic character in stream-wise direction means that the information is carried downstream only. Thus, to solve it, an initial condition is necessary (a distribution of velocity for the cross-stream plane at $x = 0$) and we can then 'march' downstream to calculate the new profile in each step and take it as initial condition for the next step.

Whereas in the x -direction the common way of using finite difference equations to approximate the derivatives seems satisfying, it was shown in [5] that in the perpendicular direction very good results can be obtained using differentiation matrices applied on *Chebyshev-Gauss-Lobatto points* (see [9]), with the advantage of a less time consuming algorithm. In fact, to obtain the results, presented in section 4.4, only minor changes have been applied to the Matlab-code presented in [5], where also algorithms from [9] are implemented.

Considering Figure 3.4, it can be seen that the velocity of the potential flow for $x \rightarrow 0$ shows very high gradients (in fact $\lim_{x \rightarrow 0} u'_s(x) = \infty$). As we need to start at $x = 0$ with an initial guess and proceed stream-wise, theoretically an infinite number of steps in the vicinity of $x = 0$ are needed. Also the calculated shear stress at the surface according to (4.18) is theoretically infinite at $x = 0$ as m is found to be below $1/3$ for all k in the present case. The fact that we cannot satisfy this requirements in the numerical simulation, leads to an initial error, which is noticeable through oscillations of the solution. Therefore, the computational mesh in the x -direction was refined in this region using 200 steps with a step size of 10^{-40} on the beginning of the calculation, whereby the rest was analyzed with a step size of 10^{-3} . Some refinement was also needed in vicinity of the curvature jump at $x = 1$ to derive the figures shown in section 4.4 (step size 10^{-4}). Both refinements were done locally and thus the originally homogenous mesh in x -direction used for the analysis was at least piece-wise homogeneous in the present case. However, the refinement in the x -direction could still be improved to increase the stability of the algorithm.

4 Behavior of the boundary layer

Another change in the existing code was needed to account for the sharp edge of the ramp function at $x = 0$ (initial condition). The presentation of the algorithm shown in [5] is done for a flow within a channel⁴ and therefore for the initial guess at $x = 0$ an approximation was done solving the Blasius-equation. However, for the given half-bodies the Falkner-Skan equation was more accurate as described in section 4.2.1.

Finally, to compute the differentiation matrices for the Chebyshev-Gauss-Lobatto points a simpler algorithm ('cheb'-algorithm) instead of the more general 'poldif'-algorithm was applied (both are presented in [9]).

4.4 Presentation of the results

Using the algorithm from [5], described in section 4.3 and the compound solution of the potential flow, shown in section 3.5, distributions of the wall shear stress, $\sigma(x)$, at the surface of the half-bodies and the displacement thickness, $\delta^*(x)$, of the boundary layer were derived for curvature jumps $k = (0 \div -2.8)$. The latter is relevant in higher order theory and physically meaningful as it describes the distance by which the external potential flow is displaced outwards (see [7]).

The global behavior of the boundary layer as $x \rightarrow \infty$ for the marginal half-body with $k = 0$ (continuous curvature along the whole surface) is compared in Figure 4.1 to the behavior of a boundary layer, which occurs in a flow along a flat plate $\delta_p^*(x)$. Due to the fact, that beyond $x = 1$ the thickness-function consists of a horizontal line, $x \rightarrow \infty$ implies $u'_s(x) \rightarrow 0$ and therefore, it can be seen by comparison of (4.12) and (4.20), considering (4.10), that as the present solution must converge to the Blasius solution. The logarithmic plot shows, that the slope corresponding to $\delta^*(x)$ is increasing slightly beyond $x = 1$, but to observe an evident convergence of the solution we would have to increase the calculated domain significantly.

The results⁵ for different k are shown in Figures 4.2 to 4.4 whereas Figure 4.5 shows the region of interest in the vicinity of the curvature jump at $x = 1$.

⁴Obviously, considering the Matlab-code shown in [5], also the input/output arguments and the definition of the potential velocity were changed appropriately to the present problem.

⁵Note, that for a better orientation a uniform color code is used for different k throughout this section.

4 Behavior of the boundary layer

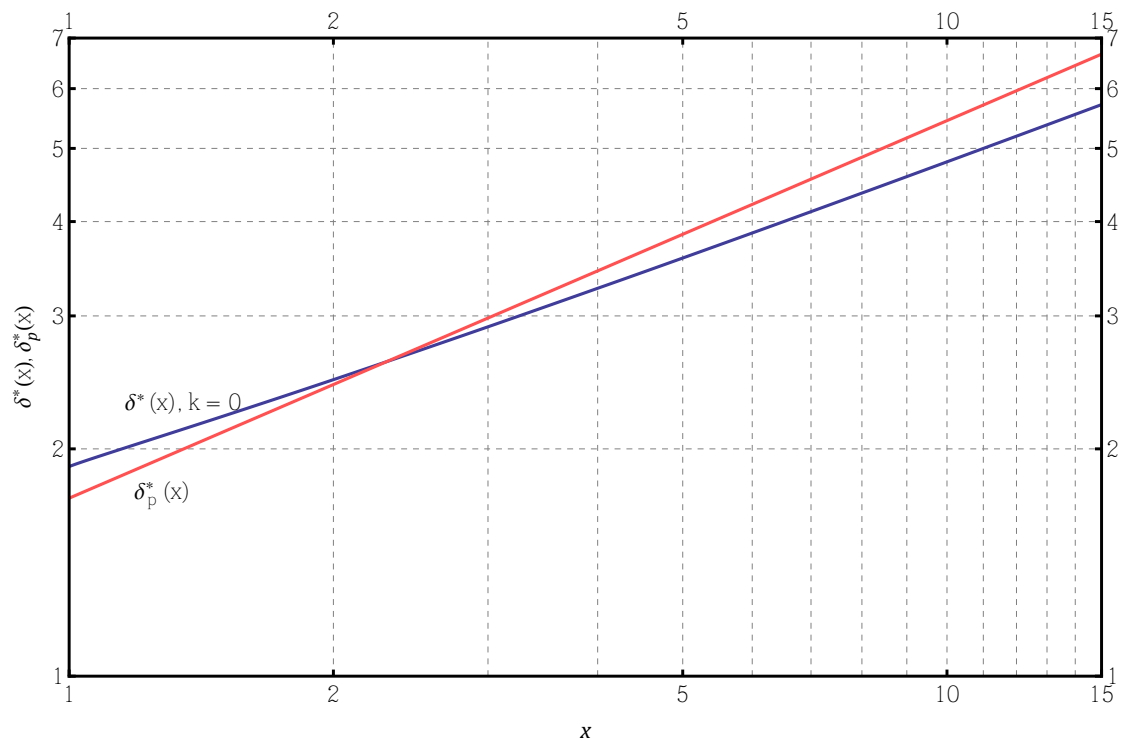
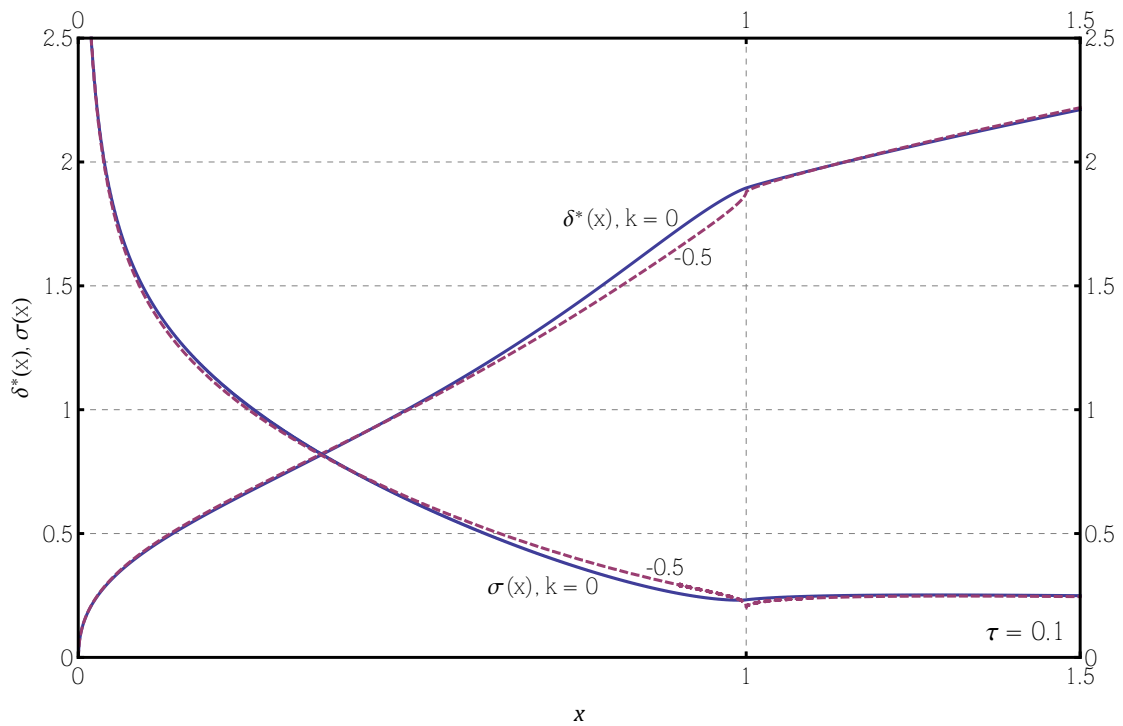
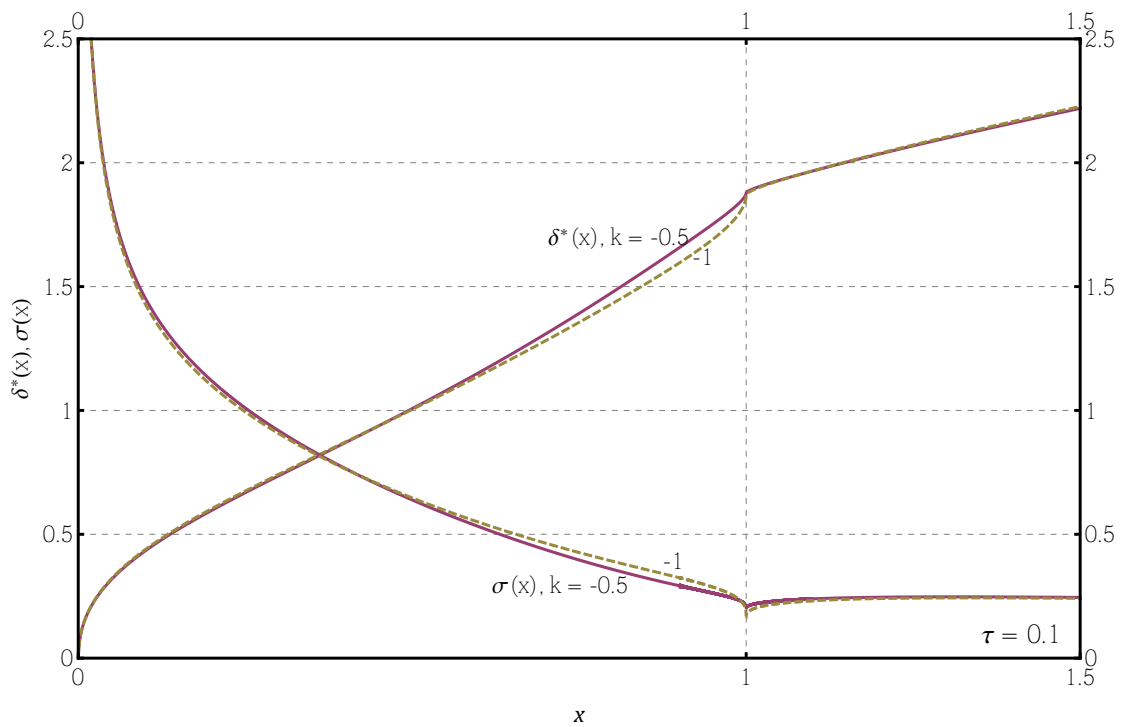


Figure 4.1: Behaviour of the boundary layer for a half-body with a continuous curvature of the surface and for a flat plate.

4 Behavior of the boundary layer



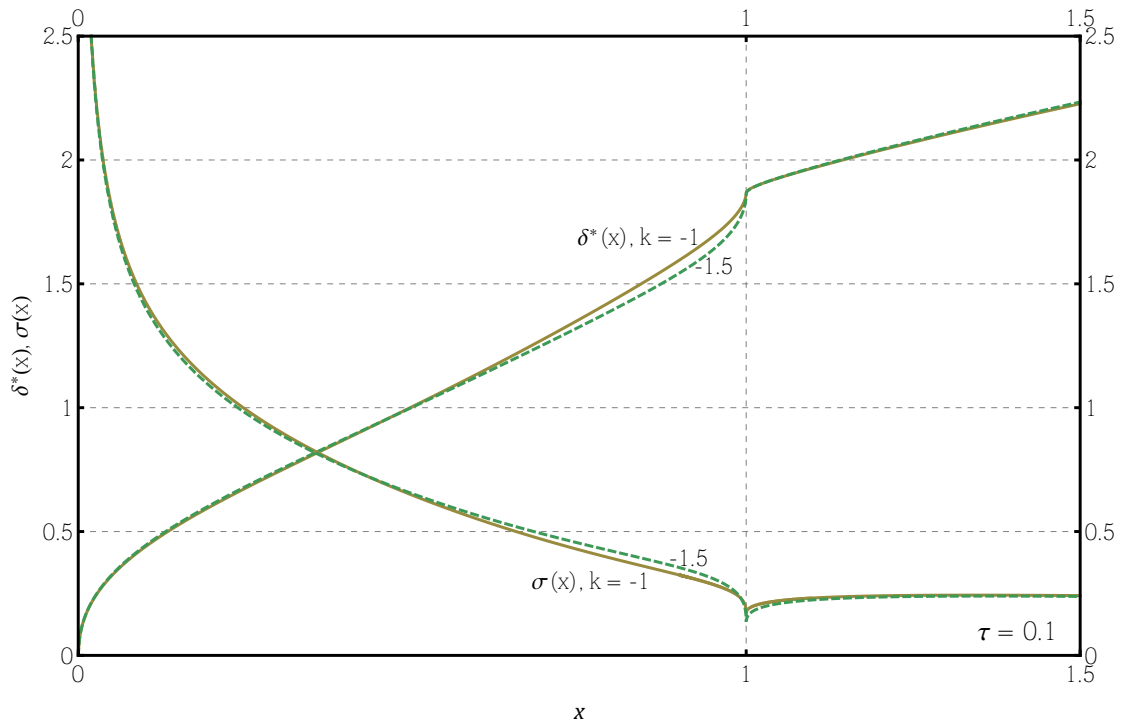
(a) $k = 0$ (solid line), $k = -0.5$ (dashed line)



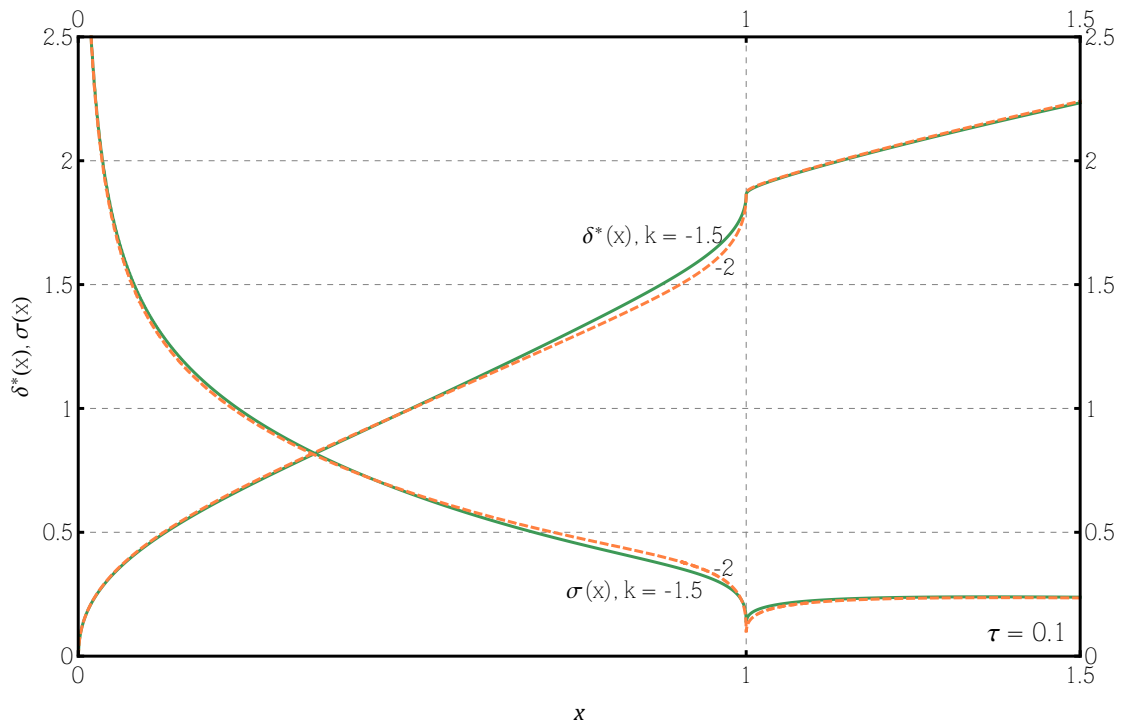
(b) $k = -0.5$ (solid line), $k = -1$ (dashed line)

Figure 4.2: Wall shear stress $\sigma(x)$ and displacement thickness $\delta^*(x)$ for different k , $\tau = 0.1$.

4 Behavior of the boundary layer



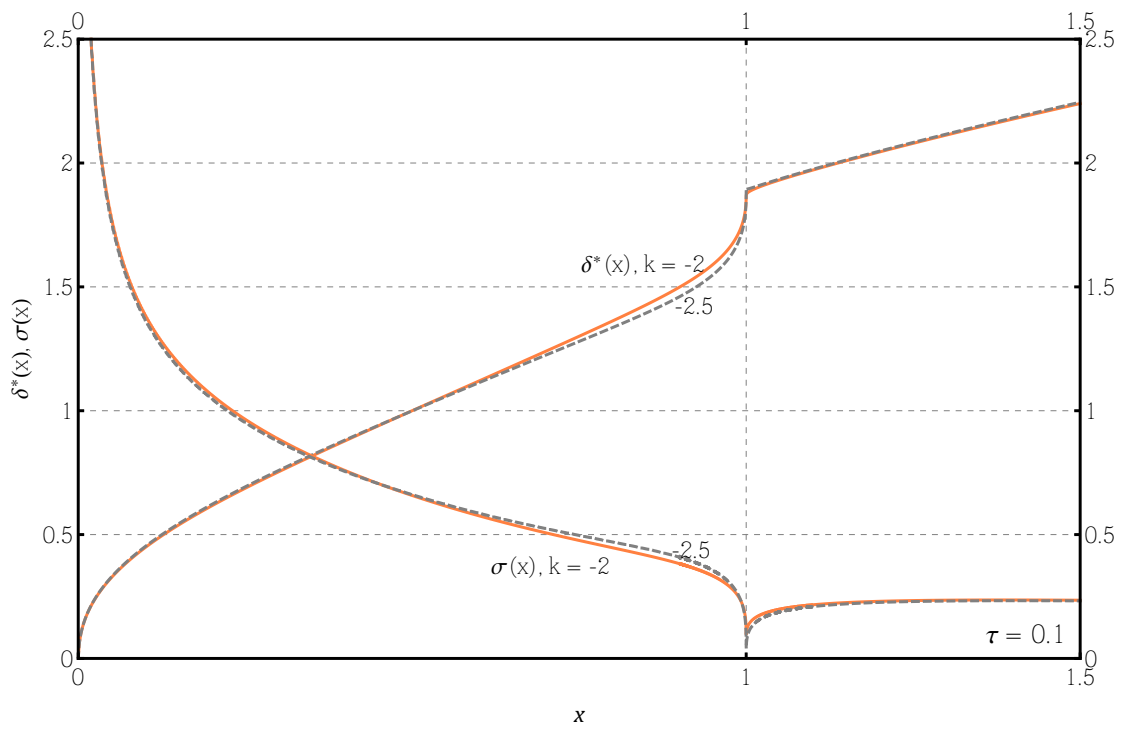
(a) $k = -1$ (solid line), $k = -1.5$ (dashed line)



(b) $k = -1.5$ (solid line), $k = -2$ (dashed line)

Figure 4.3: Wall shear stress $\sigma(x)$ and displacement thickness $\delta^*(x)$ for different k , $\tau = 0.1$.

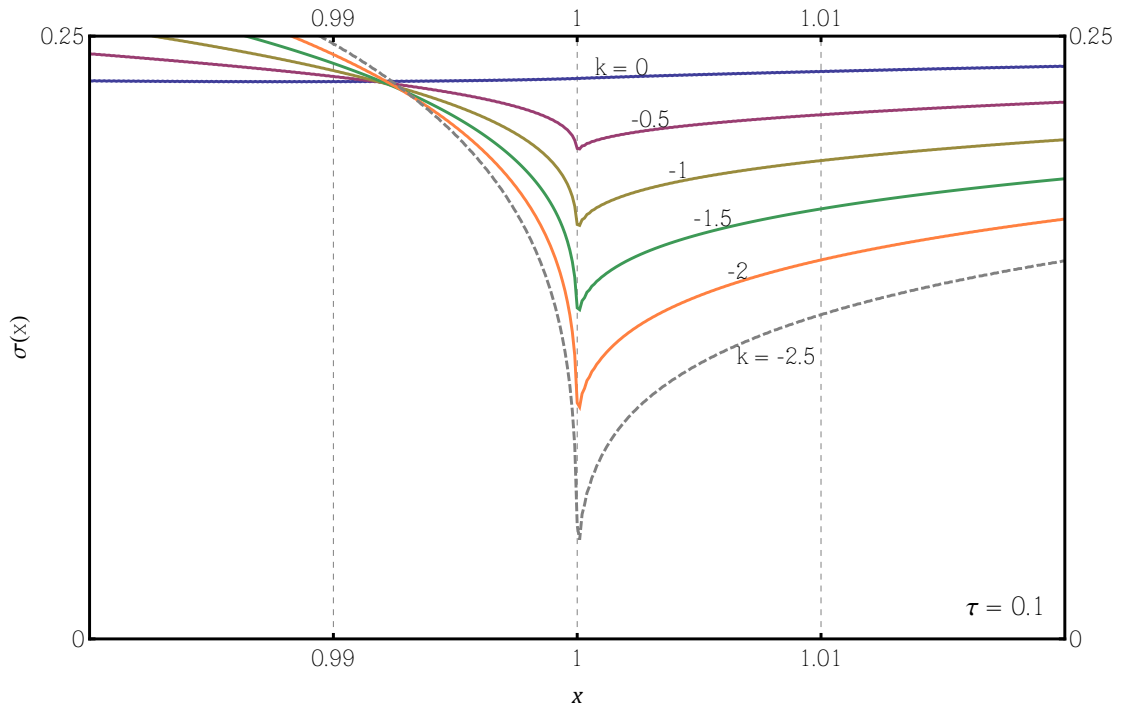
4 Behavior of the boundary layer



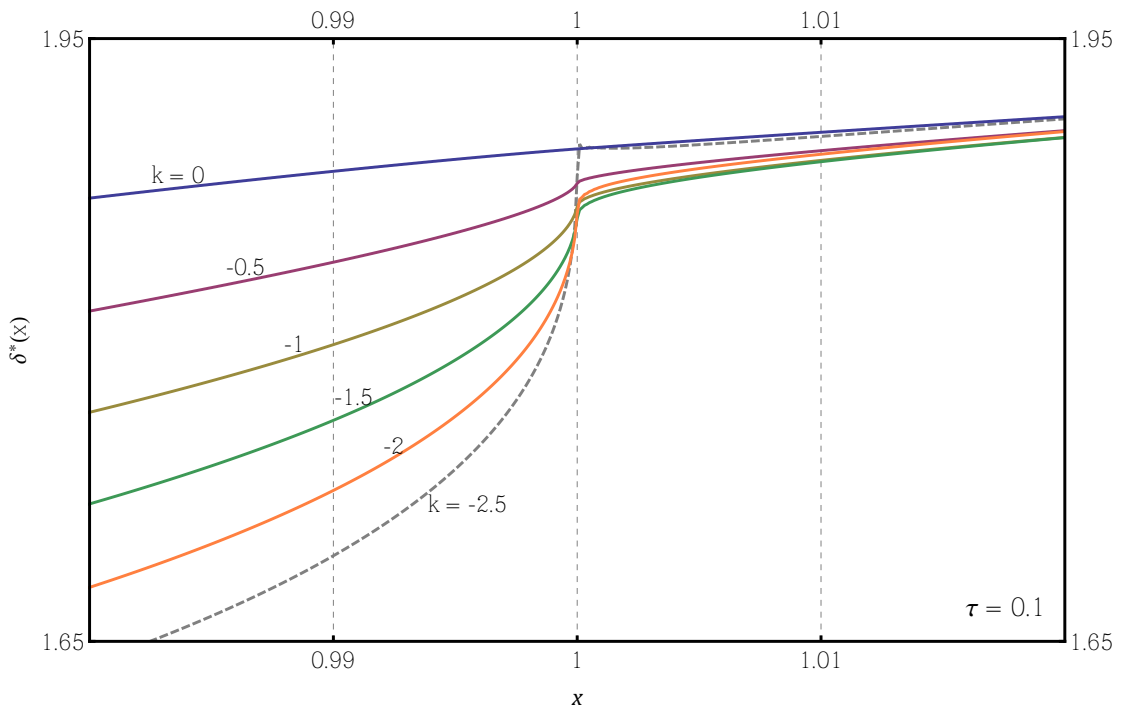
(a) $k = -2$ (solid line), $k = -2.5$ (dashed line)

Figure 4.4: Wall shear stress $\sigma(x)$ and displacement thickness $\delta^*(x)$ for different k , $\tau = 0.1$.

4 Behavior of the boundary layer



(a) Wall Shear Stress $\sigma(x)$



(b) Displacement thickness of the boundary layer $\delta^*(x)$

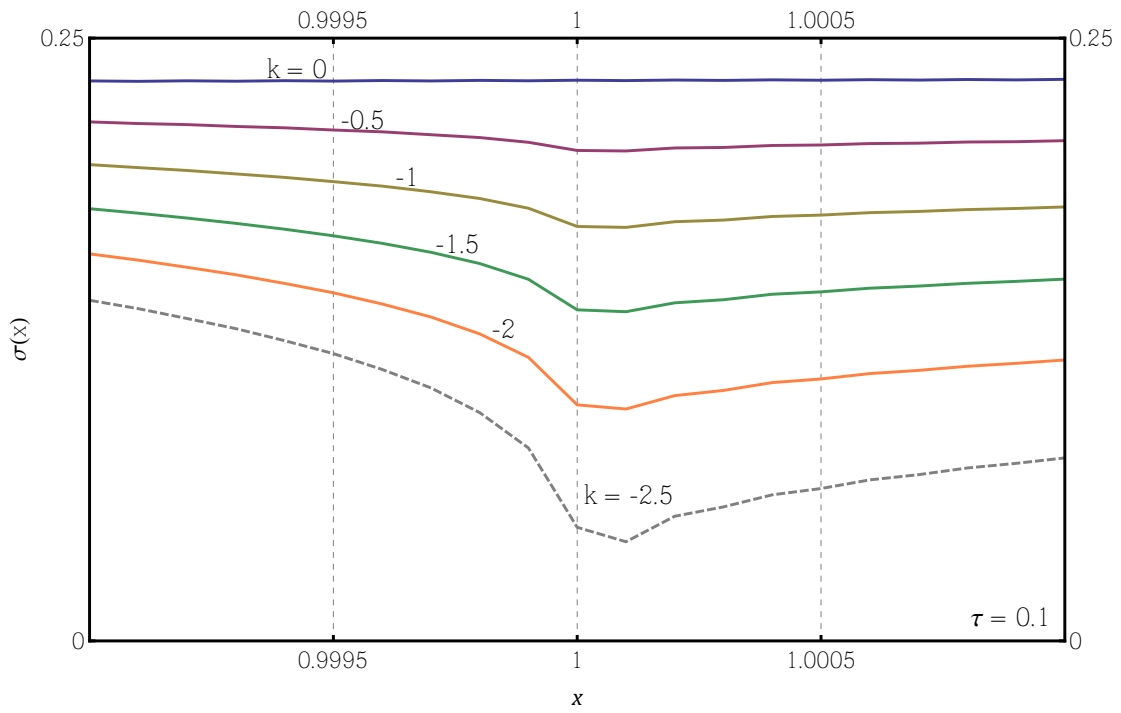
Figure 4.5: Immediate vicinity of the curvature jump for different k , $\tau = 0.1$.

4 Behavior of the boundary layer

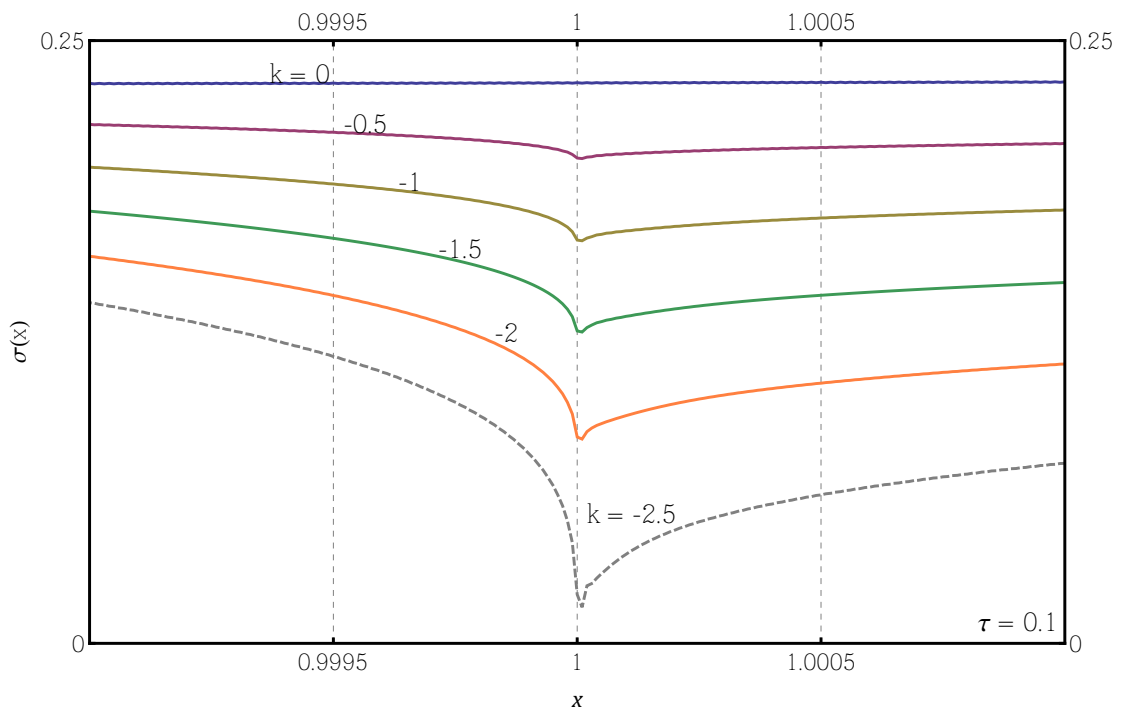
It can be seen by comparison of the different curves that a Goldstein-singularity occurring at $x = 1$, visible through a vertical tangent, is more evident as $k \rightarrow -\infty$. Although, it seems that for a small discontinuity, the slope at $x = 1$ is rather modest instead of infinite, a refinement of the mesh in x -direction shows that the singularity occurs independently of the magnitude of the curvature discontinuity. It can be seen by comparison of Figure 4.6(a) and Figure 4.6(b), showing the shear stress for different k , that it is more evident the smaller the step size is. Obviously, $\sigma(1) \rightarrow 0$ for an infinitely fine mesh. It is essential to keep in mind, that the numerical values of $\sigma(x)$ and $\delta(x)$ at $x = 1$ and in its immediate proximity cannot be interpreted as a valid approximation for the real values any more. The occurrence of the Goldstein-singularity indicates a break-down of the classical boundary layer theory. At this point the assumption of a prescribed external, frictionless flow independent of the boundary layer is violated. Moreover, the presented classical theory represents a concept which is incapable of prediction of phenomena like boundary layer separation.

The analysis of discontinuities in the surface curvature beyond $k = -2.8$ led to a break-down of the algorithm due to negative values of the wall shear stress and thus to negative 'exitflags' of the solver, which means, that the returned values were not trustworthy any more. In the case of $k = -2.8$, the algorithm terminated beyond $x = 1$ only when the number of iterations was exceeded, which explains the oscillations visible in Figure 4.7 showing this limiting case. Also the oscillations due to the initial error increased with increasing curvature as described in section 4.3.

4 Behavior of the boundary layer



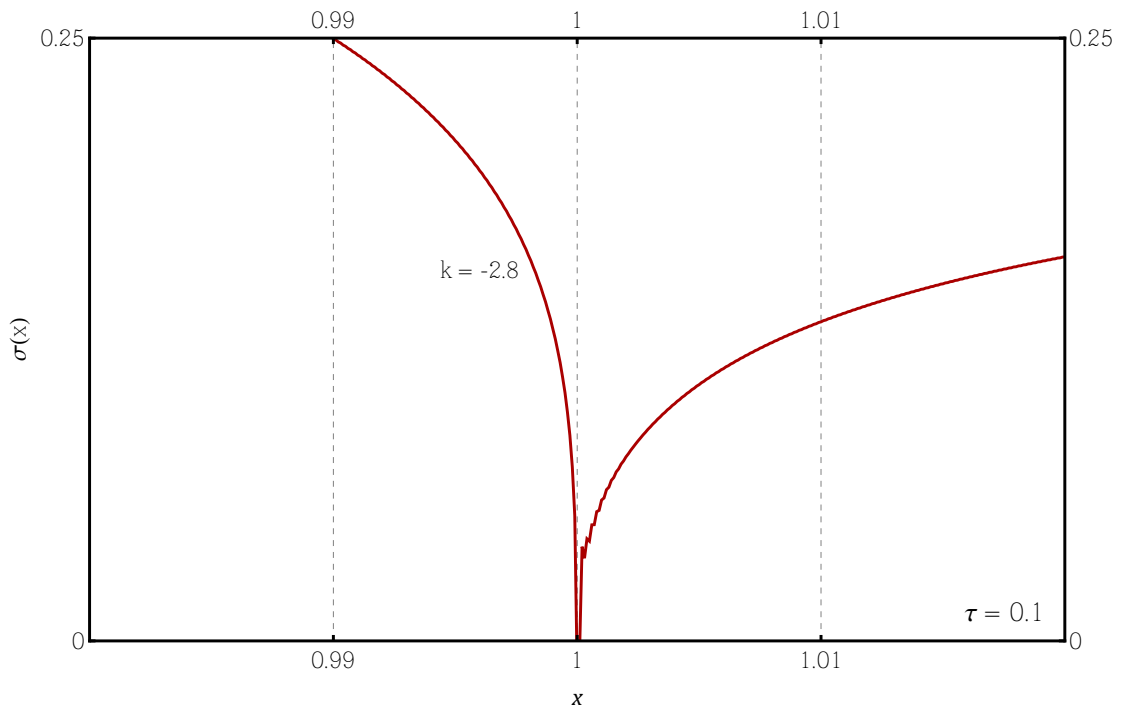
(a) Step size: 10^{-4}



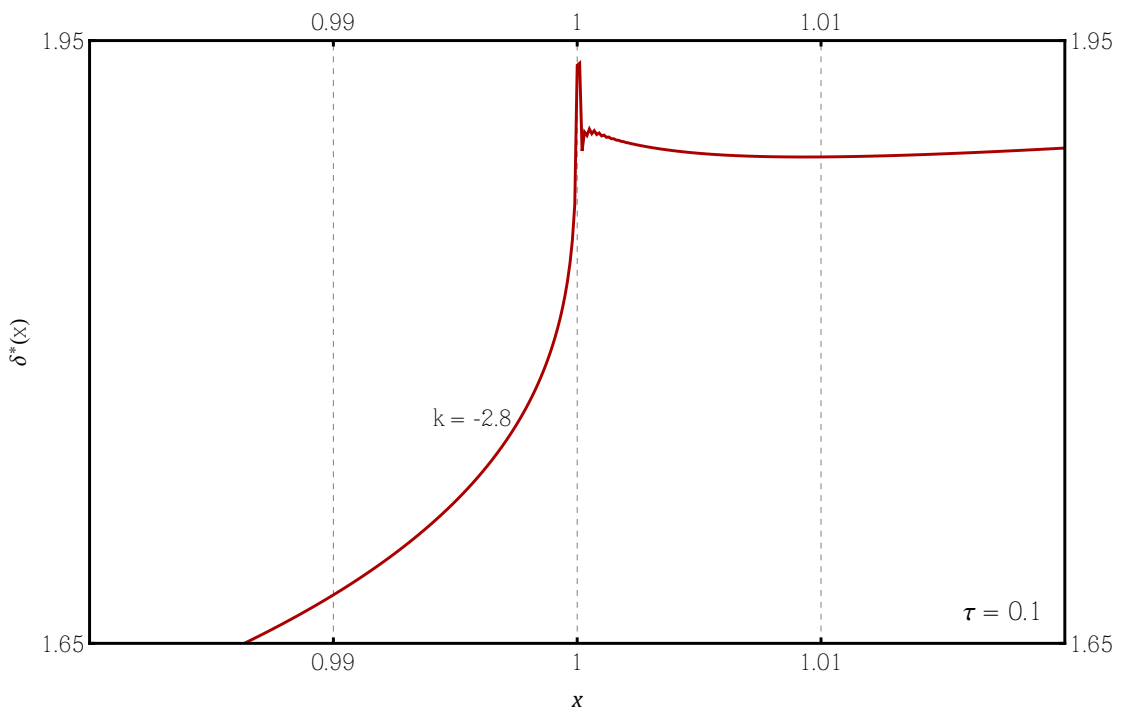
(b) Step size: 10^{-5}

Figure 4.6: Goldstein-singularity for different k and different step-size in vicinity of $x = 1$, $\tau = 0.1$.

4 Behavior of the boundary layer



(a) Wall Shear Stress $\sigma(x)$



(b) Displacement thickness of the boundary layer $\delta^*(x)$

Figure 4.7: Immediate vicinity of the curvature jump with $k = -2.8$.

5 Conclusion and outlook

This study presents a detailed description of the computation procedure to obtain solutions for different regions of a high Reynolds number flow field around a thin body. On one hand, for the nearly frictionless flow in some distance of the wall, incompressible potential theory in the small perturbation formulation was used and on the other hand, a numerical solution of Prandtl's boundary layer equations was sought in the immediate proximity of the surface. Moreover, in vicinity of the leading edge stagnation point $x = 0$, where a singularity indicates the failure of the perturbation method, the sharp edge is approximated by a wedge. It is, furthermore, shown how to obtain analytically a potential solution, valid within this small area, and how to match it to the thin airfoil solution to obtain a universally valid approximation of the whole external flow. Varying the curvature parameter of the thickness-function, different magnitudes of a curvature jump at the surface of the analyzed body, beginning at zero (continuous curvature), were investigated.

The present work revealed that, independently of its magnitude, a discontinuous curvature at the surface of a thin body leads to a break-down of the first order boundary layer theory. Although this result may not be extremely surprising, it outlines the importance of the interaction between the surrounding, inviscid flow and the viscous boundary layer in the case of a curvature jump. To account for this character of the flow further studies are needed. It will be necessary to find an appropriate scaling for the region of strong viscous interaction (presumably a triple-deck problem) and to associate the magnitude of the curvature jump to the Reynolds number to be able to observe phenomena like flow separation.

Extending the study into the supersonic flow regime and therefore accounting for compressibility effects will finally show, how to exploit the investigated effects of a curvature jump to improve the design of smart structures like adaptive aircraft wings providing high lift performance.

Moreover, through the possibility of comparison, the theoretical results will reference the accuracy of numerical simulations provided by advanced computational fluid dynamics (CFD) algorithms.

Bibliography

- [1] Braun S., *Recent developments in the asymptotic theory of separated flows. Leverhulme lectures*, Lecture notes, Manchester Institute of Mathematics Sciences, eprints 2006:226, 2006, <http://eprints.ma.man.ac.uk/656/>.
- [2] Cousteix J., Mauss J., *Asymptotic Analysis and Boundary Layers*, Springer, 2007.
- [3] Herwig H., *Strömungsmechanik, Eine Einführung in die Physik und die mathematische Modellierung von Strömungen*, 2nd ed., Springer, 2006.
- [4] Heuser H., *Gewöhnliche Differentialgleichungen, Einführung in Lehre und Gebrauch*, 6th ed., Vieweg+Teubner, 2009.
- [5] Hofmann L., *Lösung der Grenzschichtgleichungen mittels Chebyshev-Differentiationsmatritzen*, Bachelor's thesis, Vienna University of Technology, 2014.
- [6] Ruban A.I., Gajjar J.S.B., *Fluid Dynamics, Part I, Classical Fluid Dynamics*, Oxford University Press, 2014.
- [7] Schlichting H., Gersten K., *Grenzschicht-Theorie*, 9th ed., Springer, 1997.
- [8] Schneider W., *Mathematische Methoden der Strömungsmechanik*, Vieweg, 1978.
- [9] Trefethen L.N., *Spectral Methods in Matlab*, Society for Industrial and Applied Mathematics, 2000.
- [10] Van Dyke M., *Perturbation Methods in Fluid Mechanics*, annotated ed., The Parabolic Press, 1975.